ALMA Calibration Loads
Test Report

FEND-40.06.04.00-016-D-REP

Version: D

Status: Released

2010-09-14

Prepared By: Name and Signature	Organization	Date
P. Yagoubov A. Murk	ESO IAP, University of Bern	
Revised & Approved **Name(s) and Signature(s)**	**Organization**	**Date**
P. Yagoubov	ESO	
Approved By **Name(s) and Signature(s)**	**Organization**	**Date**
Released By ESO		
Name and Signature	**Organization**	**Date**
G.H. Tan	ESO	

Change Record

Version	Date	Affected Section(s)	Change request #	Reason/remarks
A	2009-11-11	All		First document issue
B	2010-04-30	5	-	Added chapters 5.2-5.4
C	2010-06-15	5.4	-	Chapter 5.4 added measurements with ambient/hot loads on a load scanner
D	2010-09-14	2.3 4.2		Production Loads Test results added

TABLE OF CONTENTS

FIGURES

1. INTRODUCTION

1.1. Scope

This report summarizes the test results of the Hot Calibration Load (HCL) and Ambient Calibration Loads (ACL) prototypes for ALMA, at the moment of the Critical Design Review.
The purpose of these tests was to verify that the Calibration Loads design [RD3] meets the requirements specified in the ACD Technical Specification Document [AD1].

1.2. Applicable Documents List

The following documents are part of this document to the extent specified herein. If not explicitly stated differently, the latest issue of the document is valid.

Reference	*Document title*	*Document ID*
[AD1]	Amplitude Calibration Device: Technical Specifications	ALMA-40.06.00.00-009-B-SPE

1.3. Reference Documents List

The following documents contain additional information and are referenced in this document.

Reference	*Document title*	*Document ID*
[RD1]	ALMA Product Tree	ALMA-80.03.00.00-001-N-LIS
[RD2]	ALMA Calibration Device Prototype Calibration Load Test Report	FEND-40.06.04.00-005-A-REP
[RD3]	ALMA Calibration Loads Design Report	ALMA-40.06.04.00-017-B-DSN
[RD4]	Material Measurements and Raytracing Simulations for ALMA Conical Calibration Targets	ALMA-40.06.04.00-021-A-REP
[RD5]	ALMA Calibration Loads Structural and Thermal Analysis	ALMA-40.06.04.00-019-B-DSN
[RD6]	CFD analysis of the pre-production ALMA Hot Calibration Target	ALMA-40.06.04.00-020-A-REP

1.4. Acronyms

ACL	Ambient Calibration Load
ACD	Amplitude Calibration Device
AD	Applicable Document
ALMA	Atacama Large Millimeter Array
CDR	Critical Design Review
CIDL	Configuration Ítems Data List
DAC	Digital to Analog Converter
ESO	European Organisation for Astronomical Research in the Southern Hemisphere
GF	Glass Fibre
GFRP	Glass Fibre Reinforced Polymer
HCL	Hot Calibration Load
HVAC	Heating, Ventilation, Air-conditioning
ICD	Interface Control Document
RD	Reference Document
TBC	To Be Confirmed
TBD	To Be Determined

2. RF PERFORMANCE

2.1. Measurements setup

The test setup has been described previously in the pre-prototype test report [RD2].

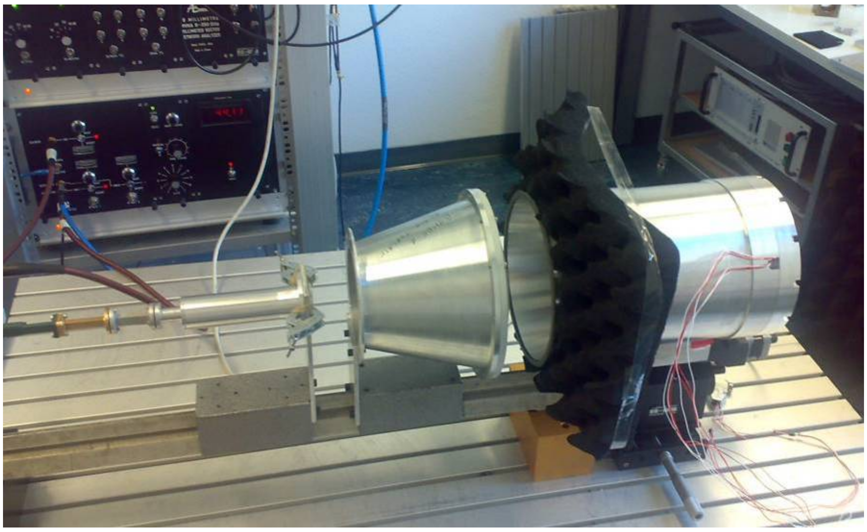

Figure 2-1 ALMA Band 1 feed horn and lens antenna in front of the ACL.

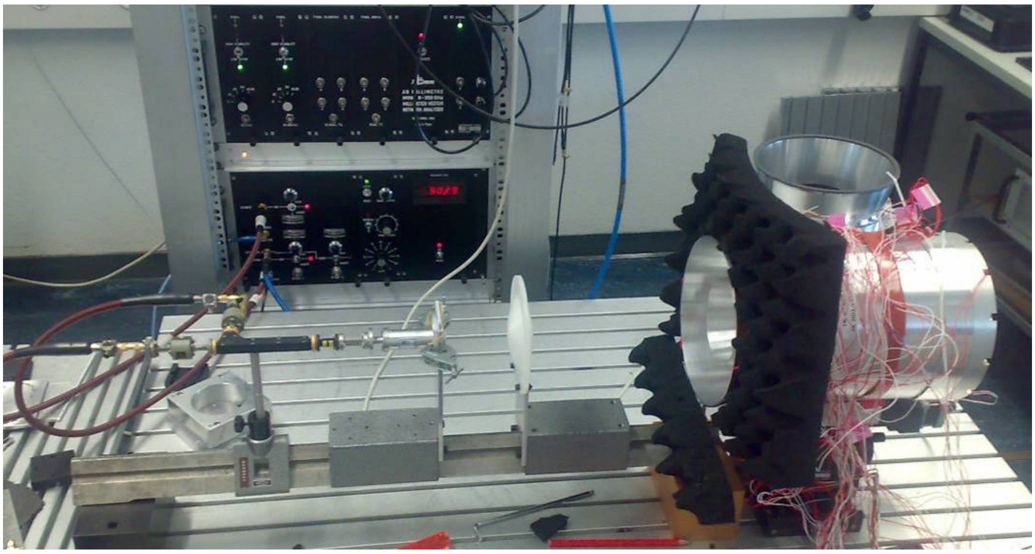

Figure 2-2 ALMA Band 2 feed horn and lens antenna in front of the HCL. S11 measurement using an ABmm VNA and directional waveguide coupler.

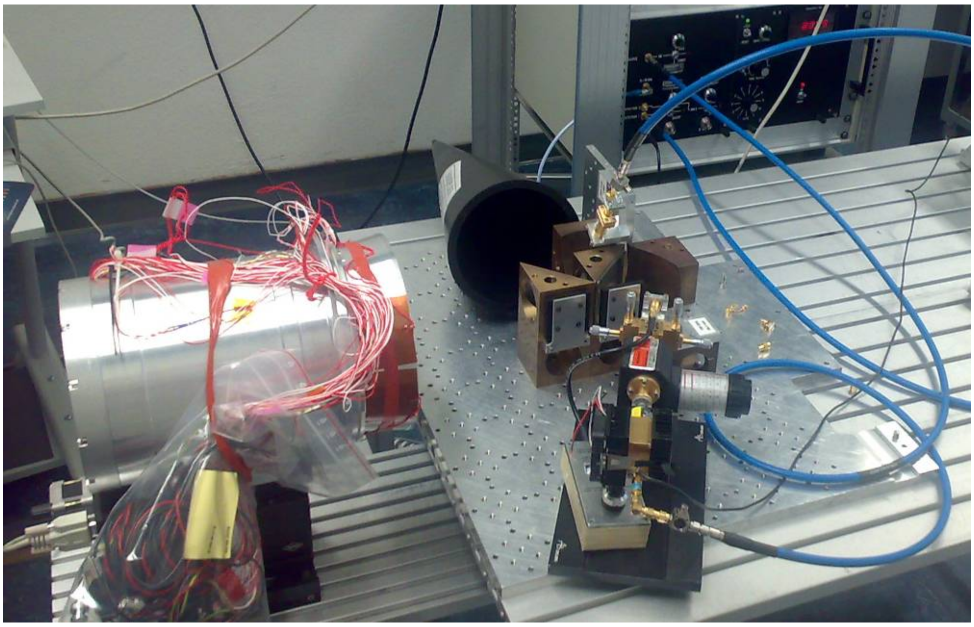

Figure 2-3 Quasi-optical directional coupler for measuring the HCL S11 in Band 4.

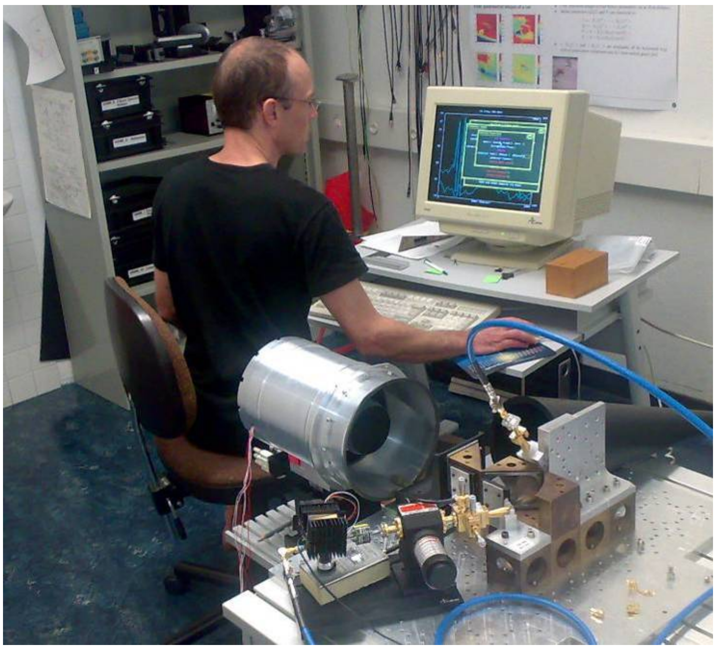

Figure 2-4 ACL in the quasi-optical S11 test setup.

2.2. Results

This section presents results of the ACL and HCL prototypes S11 performance.

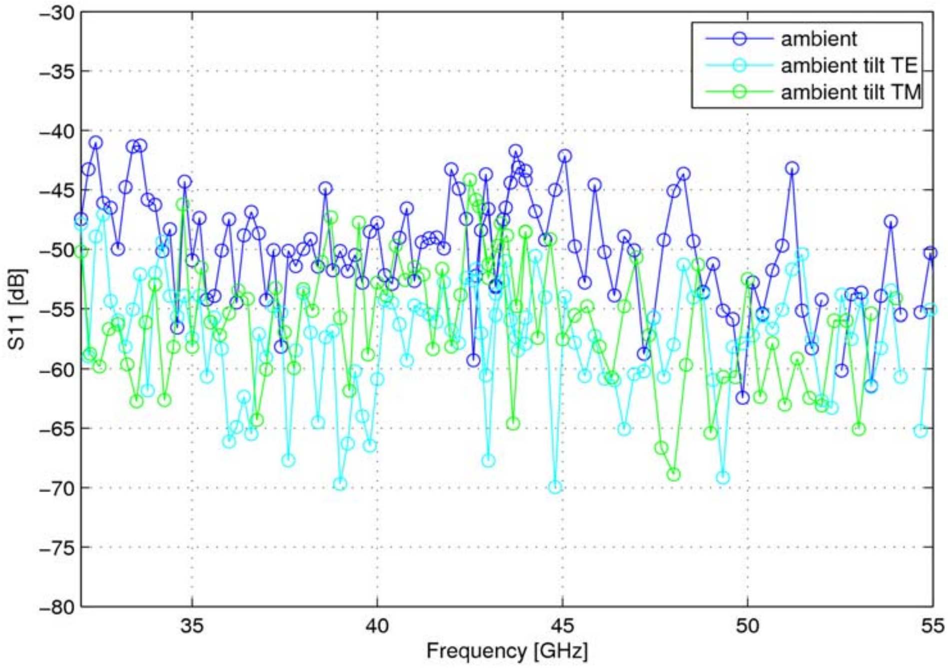

Figure 2-5 ACL in Band 1 at normal incidence and with the nominal tilt of 2.5 degrees in the two principal polarization planes.

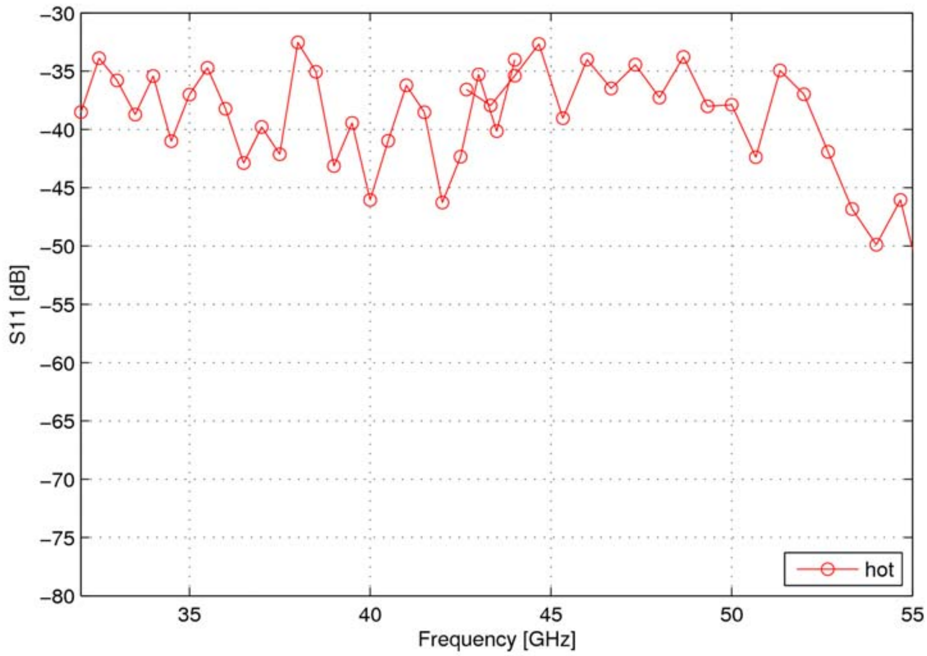

Figure 2-6 HCL in Band 1 at normal incidence.

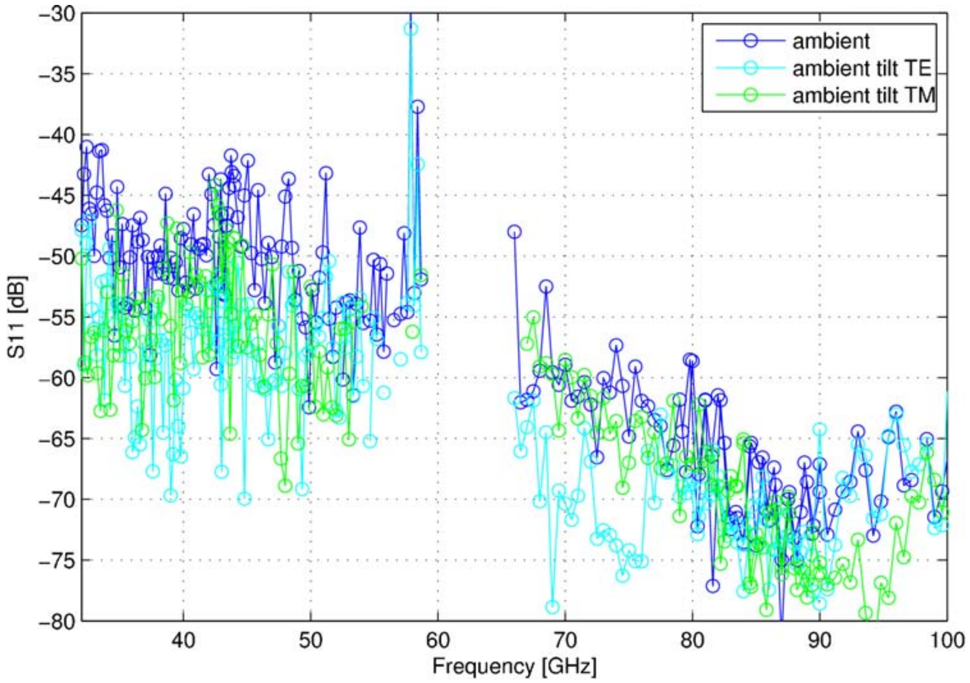

Figure 2-7 ACL in Bands 1-2 at normal incidence and with the nominal tilt of 2.5 degrees in the two principal polarization planes.

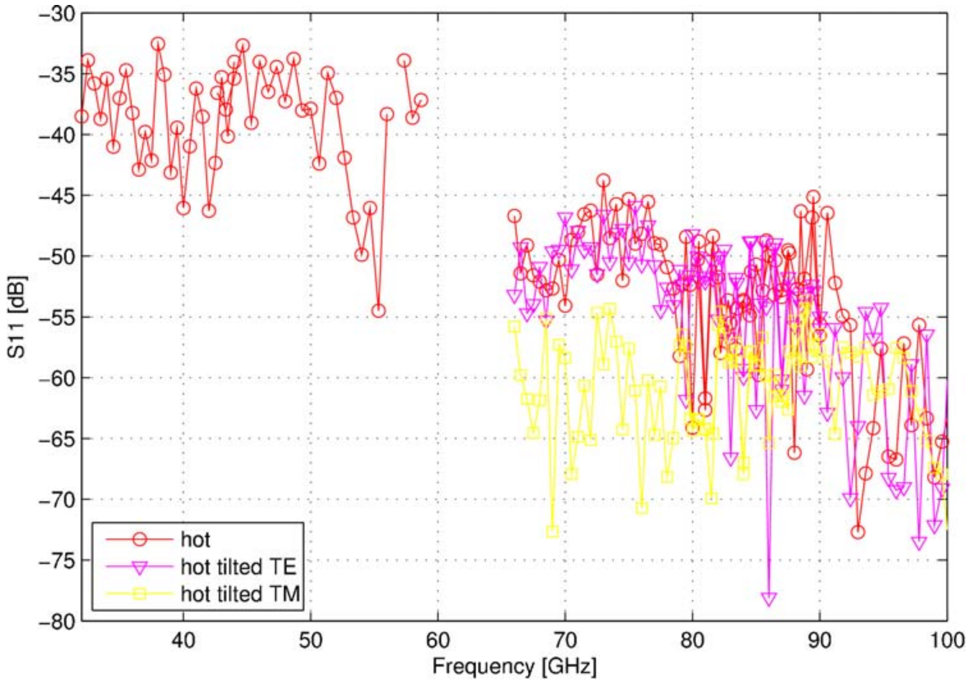

Figure 2-8 HCL in Bands 1-2 at normal incidence and with the nominal tilt of 2.5 degrees in the two principal polarization planes.

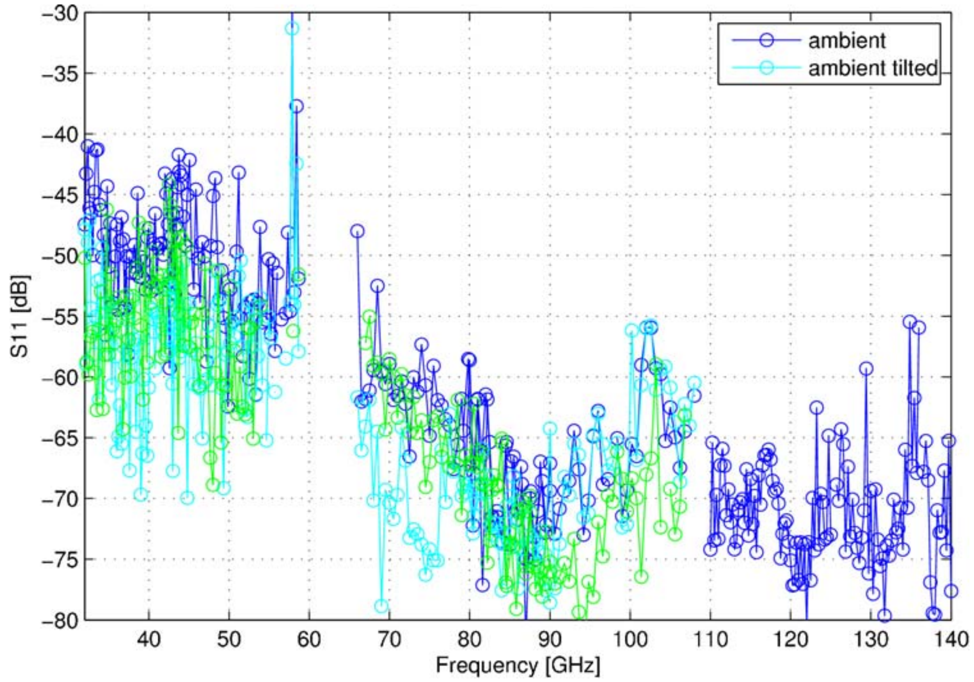

Figure 2-9 ACL in Bands 1-3 at normal incidence and with the nominal tilts..

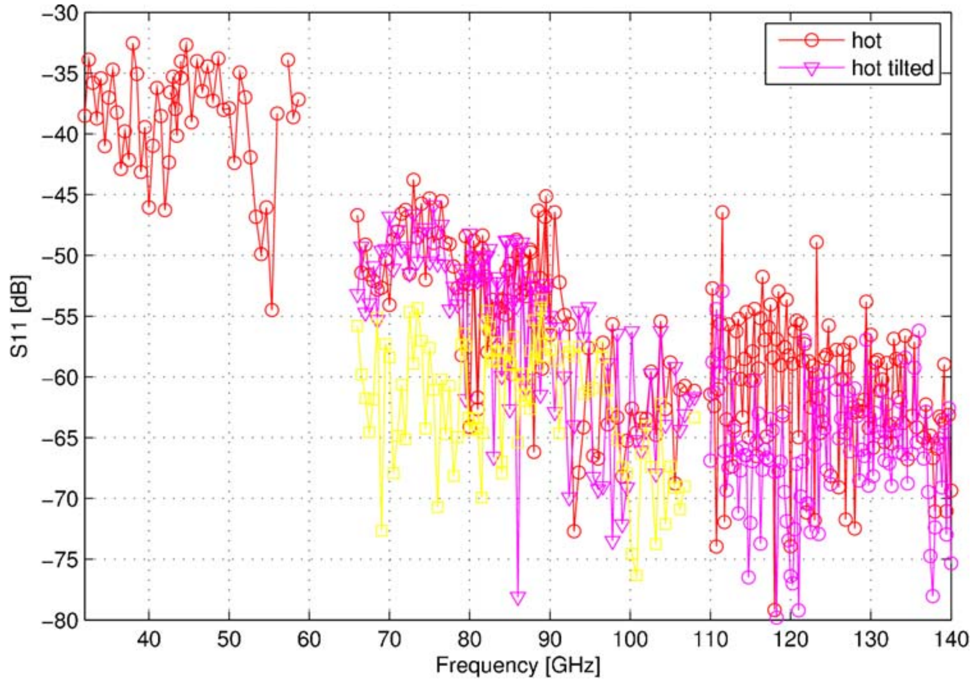

Figure 2-10 HCL in Bands 1-3 at normal incidence and with the nominal tilts.

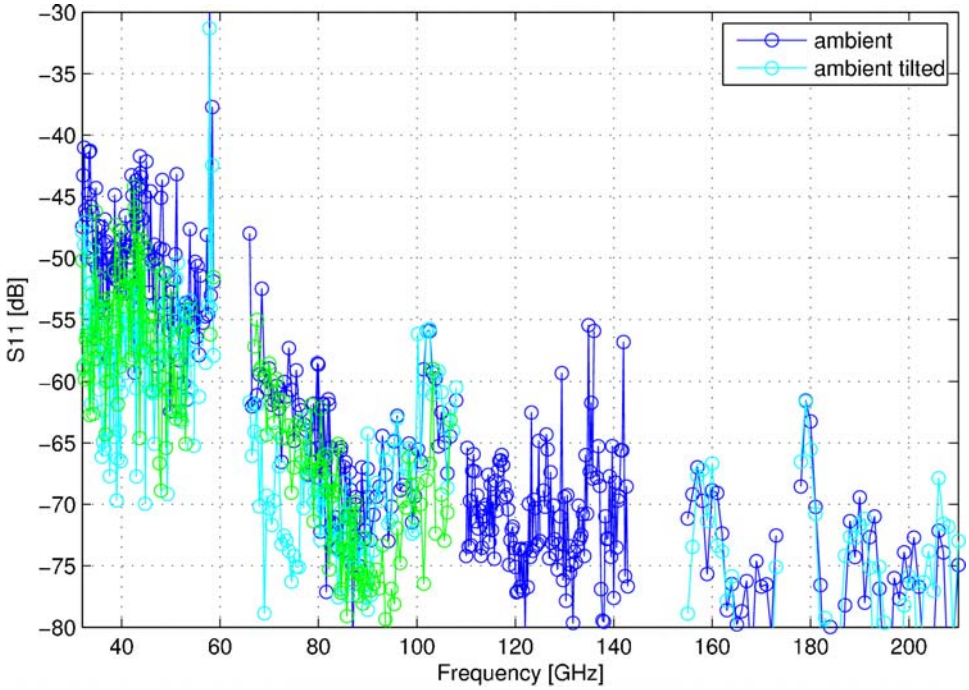

Figure 2-11 ACL in Bands 1-5 at normal incidence and with the nominal tilts.

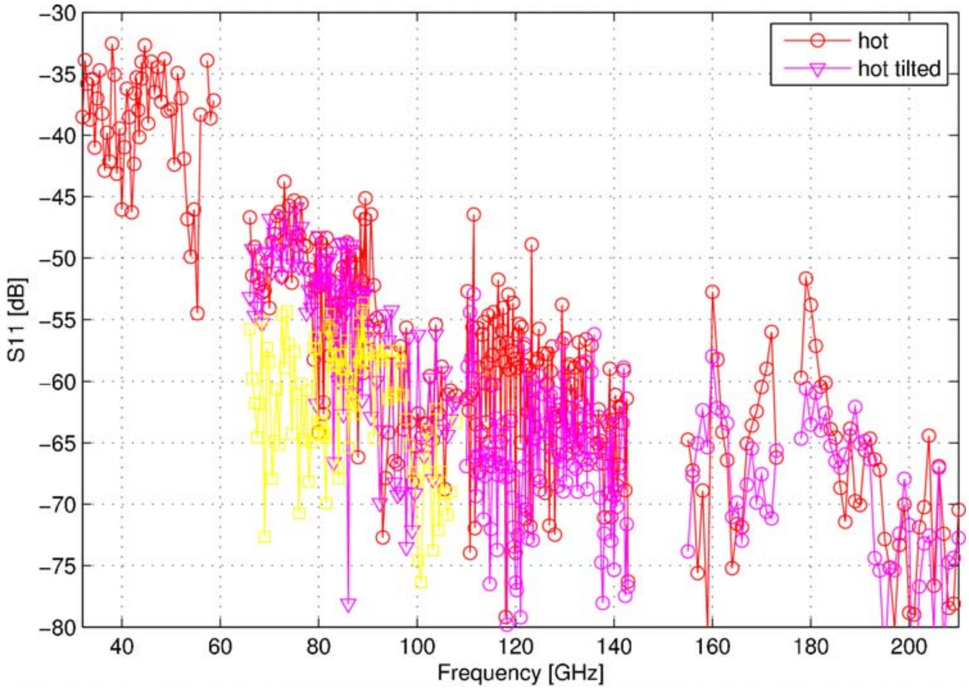

Figure 2-12 HCL in Bands 1-5 at normal incidence and with the nominal tilts.

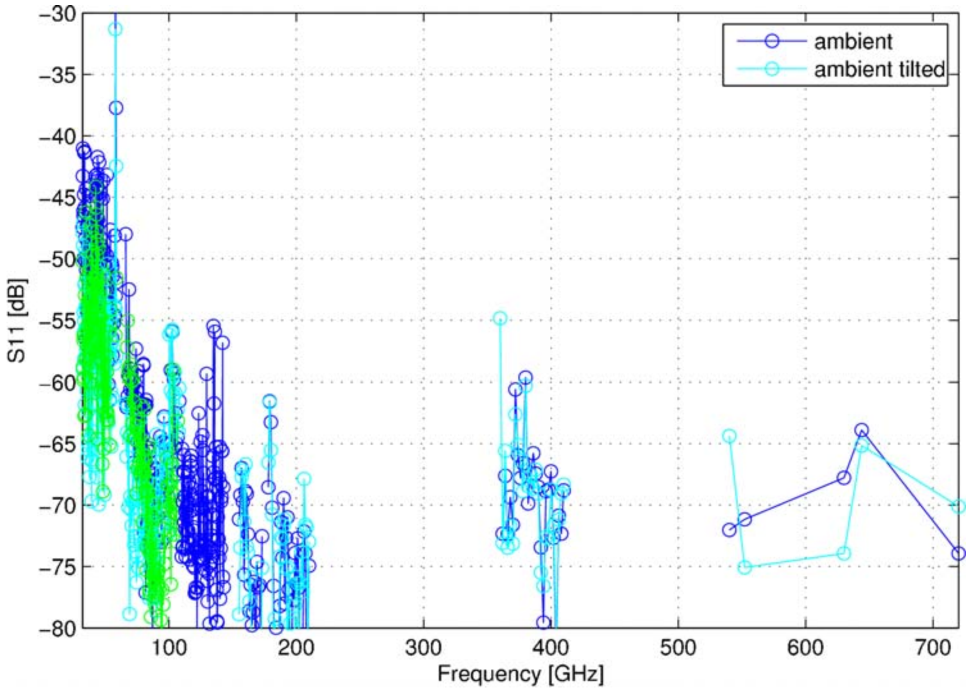

Figure 2-13 ACL in Bands 1-9 at normal incidence and with the nominal tilts.

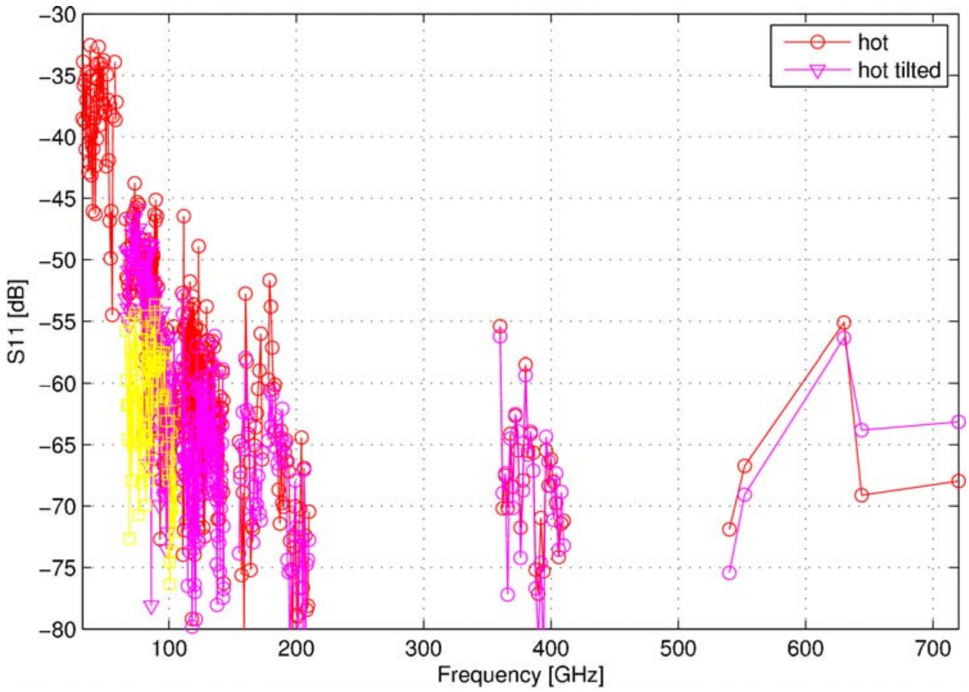

Figure 2-14 HCL in Bands 1-9 at normal incidence and with the nominal tilts.

2.3. Production Calibration Loads test results

Before going in full production, one set of ALMA Calibration Loads, HCL and ACL, fabricated by the Contractor, have been tested again using the same setup to confirm the performance of the final design, as compared to the prototypes. Because most of the modifications were potential to change the performance only at low frequencies, as change of the secondary absorber material from CR to CRS, slots in the Al backing of the main cone, rounding the edges of the secondary reflector and the inner edge of the main reflector etc, and also because the loads were well in specs for the higher frequencies, above ~120 GHz, we have limited our tests in this case to the range of ALMA Bands 1-4.

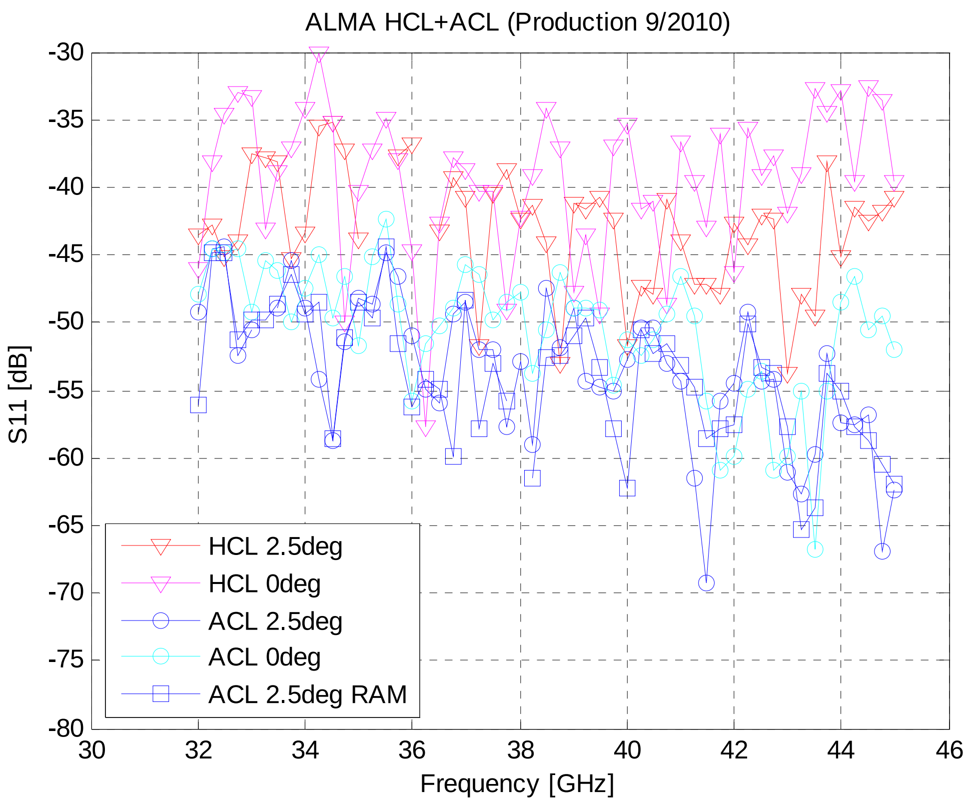

Figure 2-15 S11 results with the ALMA B1 Optics.
The HCL and ACL were tested at normal incidence (0deg) and at the nominal tilt angle of about 2.5deg. An additional measurement with Eccosorb CV absorber around the aperture (RAM) confirmed that the S11was not caused by the spillover to the mounting frame.

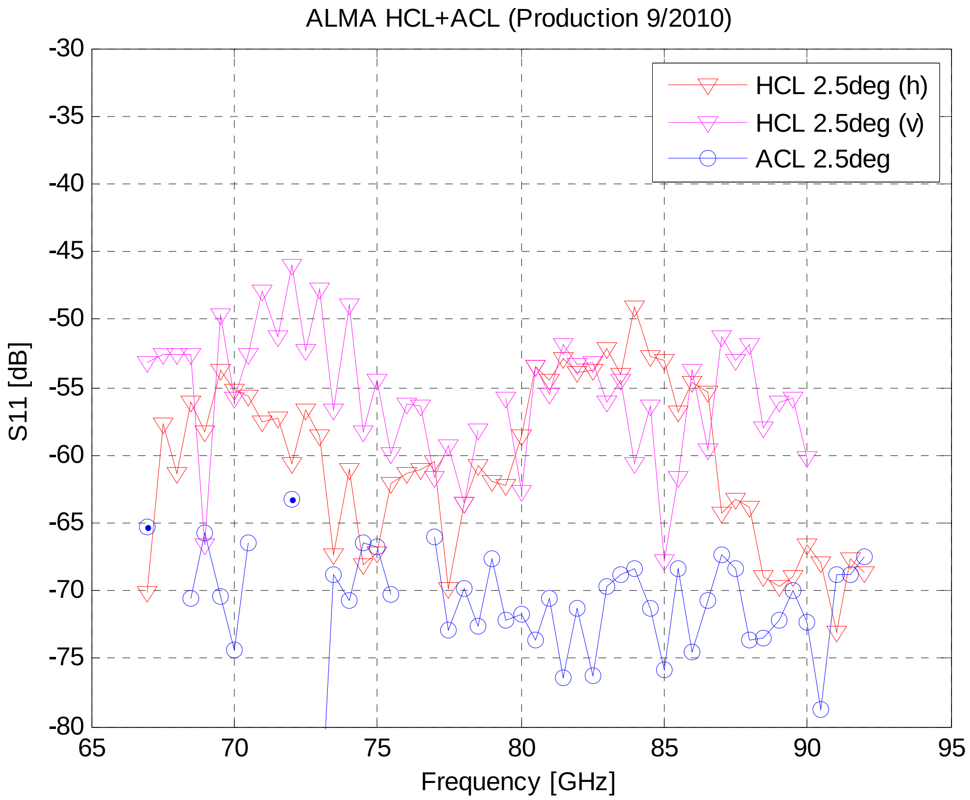

Figure 2-16 S11 results with the ALMA B2 Optics.
The HCL has been tested with the 2.5deg tilt angle in the horizontal (h) and in the vertical (v) plane to investigate the effect of the polarization (E || v).

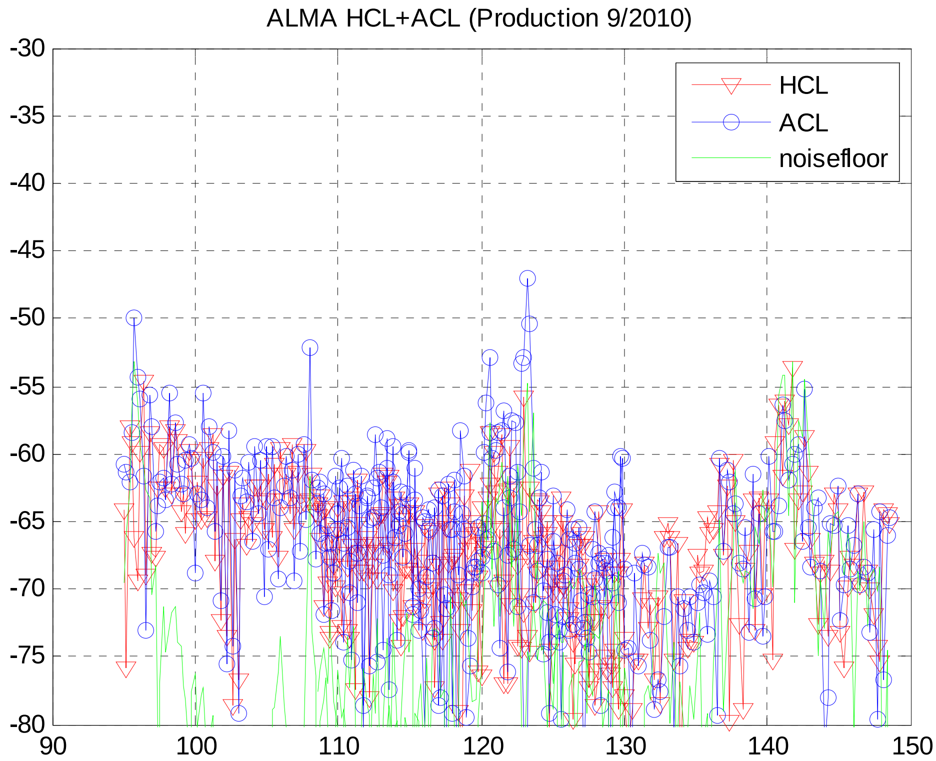

Figure 2-17 S11 results with the IAP Optics between 95-150GHz.
The green curve shows the noise oor of this measurement, which indicates the the results above 120 GHz are tilted by the sensitivity of the test setup and that the actual S11 will be lower. For that reason the increased S11 >-60dB around 120GHz and 140GHz are test artifacts because of the reduces sensitivity of the VNA in these bands.

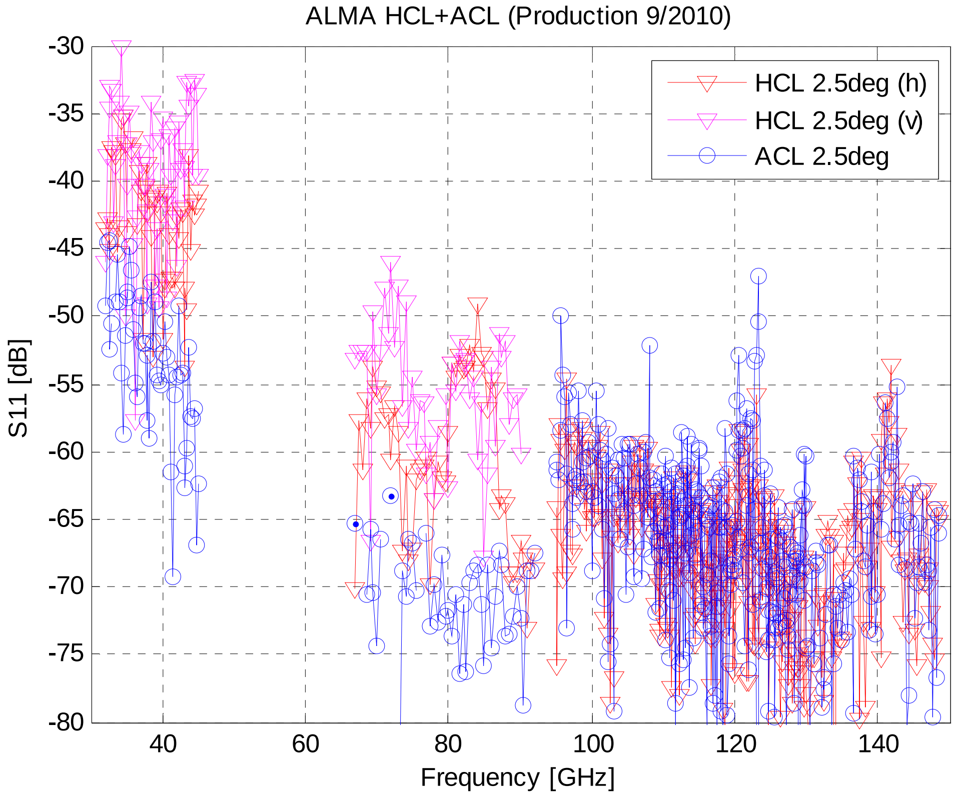

Figure 2-18 Summary of the S11 results of the production targets.

2.4. Conclusions

The coherent backscatter of the ACL and HCL conical target prototypes have been tests between 32 and 720GHz. The ACL is well below -55dB for Bands 2-9, and for bands above B3 mostly below -60dB. In Band 1 it is only in average at the -55dB level when operated at the nominal incidence angle of about 2.5 degrees, but worse at some frequencies and at normal incidence.
The HCL has a similar good performance for frequencies above 90GHz. In Band 2 it only reaches the -50dB level, and in Band 1 it is worse than -40dB.

Especially for Bands 1-3 the S11 results show significantly more structures than the initial tests ALMA-40.06.04.00-021-A-REP of the inner conical absorber and shroud because of the interference of different scattering parts of the targets, i.e. the outer and the inner absorber cavities and the rims of the shrouds. In order to improve the performance for these bands a different design with less discontinuities would be needed, for Band 1 preferably with a slightly larger overall aperture.

The performance of the tested production run targets is similar to the prototype results.

3. THERMAL PERFORMANCE

3.1. Measurements setup

The test set-up comprises two calibration targets, ACL and HCL, mounted on a common platform (calibration wheel), which can be tilted in the range -30÷+80 degrees. The axis of the calibration target is perpendicular to the mounting plate.
The tests were performed under laboratory conditions:

Temperature	25 °C (no active control)
Altitude	500 m above see level
Humidity	<60 % (no active control and monitor)
Tilt	0 deg, -30 deg, 30 deg, 60 deg
Active air flow	0 m/s, 1 m/s, 2 m/s

Calibration Loads were operated under different air flow levels and tilts to simulate actual operating conditions inside the antenna receiver cabin (high altitude was not addressed in these experiments). The test configurations are described in the following pictures. To simulate the air flow, commercial fan "ELTA" was used, with the most powerful flow settings "3", distance to the Calibration Loads assembly ~1.5 m. Air flow measured by the "Airflow TA440" anemometer close to the HCL aperture at this condition ~ 1m/s.

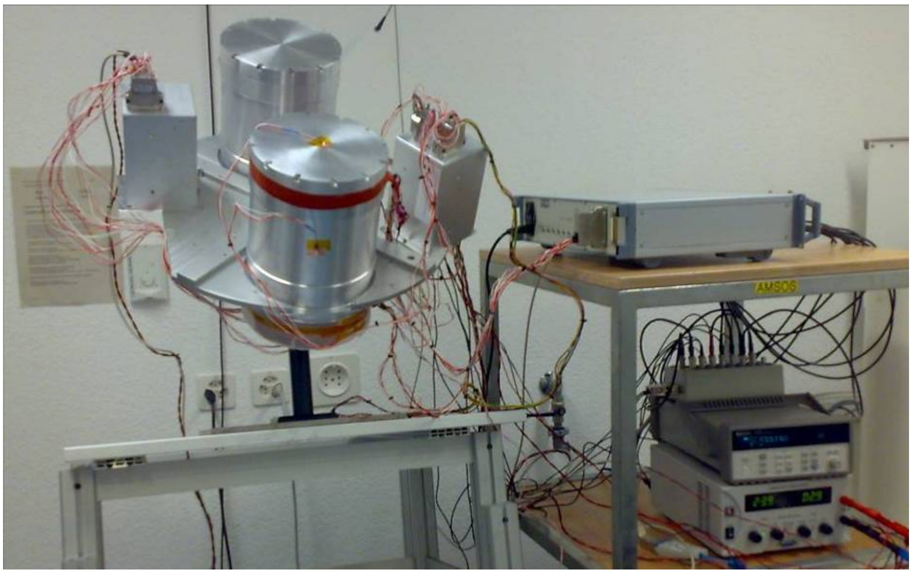

Figure 3-1 Calibration Loads, -30 deg tilt

Figure 3-2 Calibration wheel at 60 degrees tilt. Airflow simulated by "ELTA"

The following equipment was used for data acquisition and processing:

- Temperature sensors
- ACD Controllers
- Data acquisition unit
- Multimeter
- Tunable resistors

The calibration targets are equipped with their thermal control system including heaters, temperature sensors and controllers independently from the test facility [RD3]. Additional equipment was used for additional monitoring of diagnostic temperature sensors and for current and voltage measurement (determination of heater powers).
The temperature sensors were calibrated prior to use at ambient temperature (25°C) and at elevated temperature (90°C).
Three temperatures sensors, “3”, “9”, and “10” are used by MINCO controllers to set temperatures of the Main Absorber, Secondary Absorber and Main Reflector, respectively. Outputs of the MINCO controllers are also monitored by the measurement system. However, MINCO controllers in combination with their readout have not been calibrated beforehand.
There are 8 sensors read out by a standard ACD controller, those depicted by “XX(1)”.
10 extra diagnostic PT100 sensors have been installed inside the HCL to assess internal gradients of different parts. Those temperature sensors, depicted by “1-10”, are read out by the additional data logger (Agilent HP34970A) of the measurements setup.
One more ACD controller and 8 diagnostic temperature sensors have been used to measure external surface temperature of HCL, those sensors are depicted by “XX(2)”.
Temperature sensors locations are indicated in the following figures.

ACL

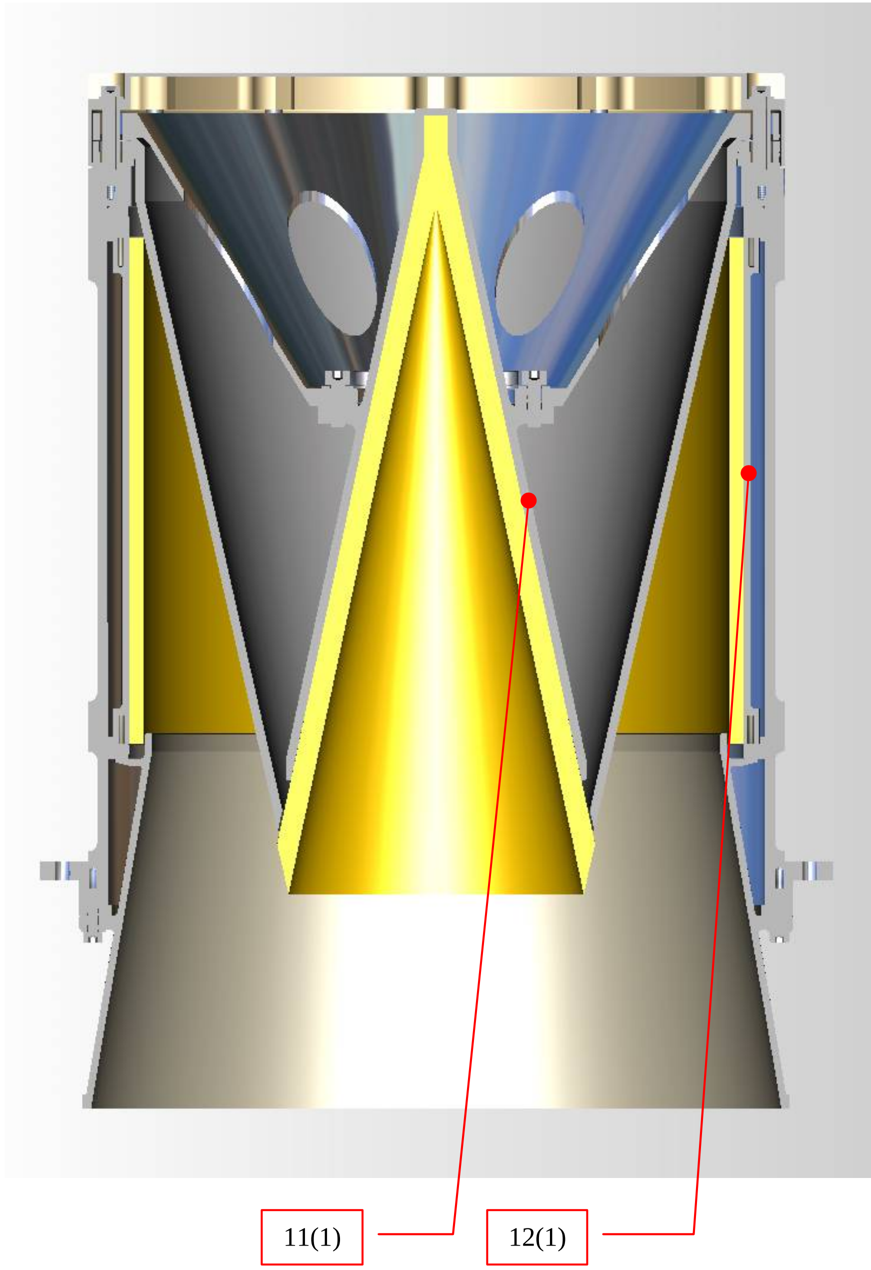

Figure 3-3 ACL temperature sensors locations

HCL

Mounted on the calibration wheel such that axis of rotation for elevation change is perpendicular to the drawing plain, rotation clockwise for positive tilts. Wires from the load are pointing towards you.

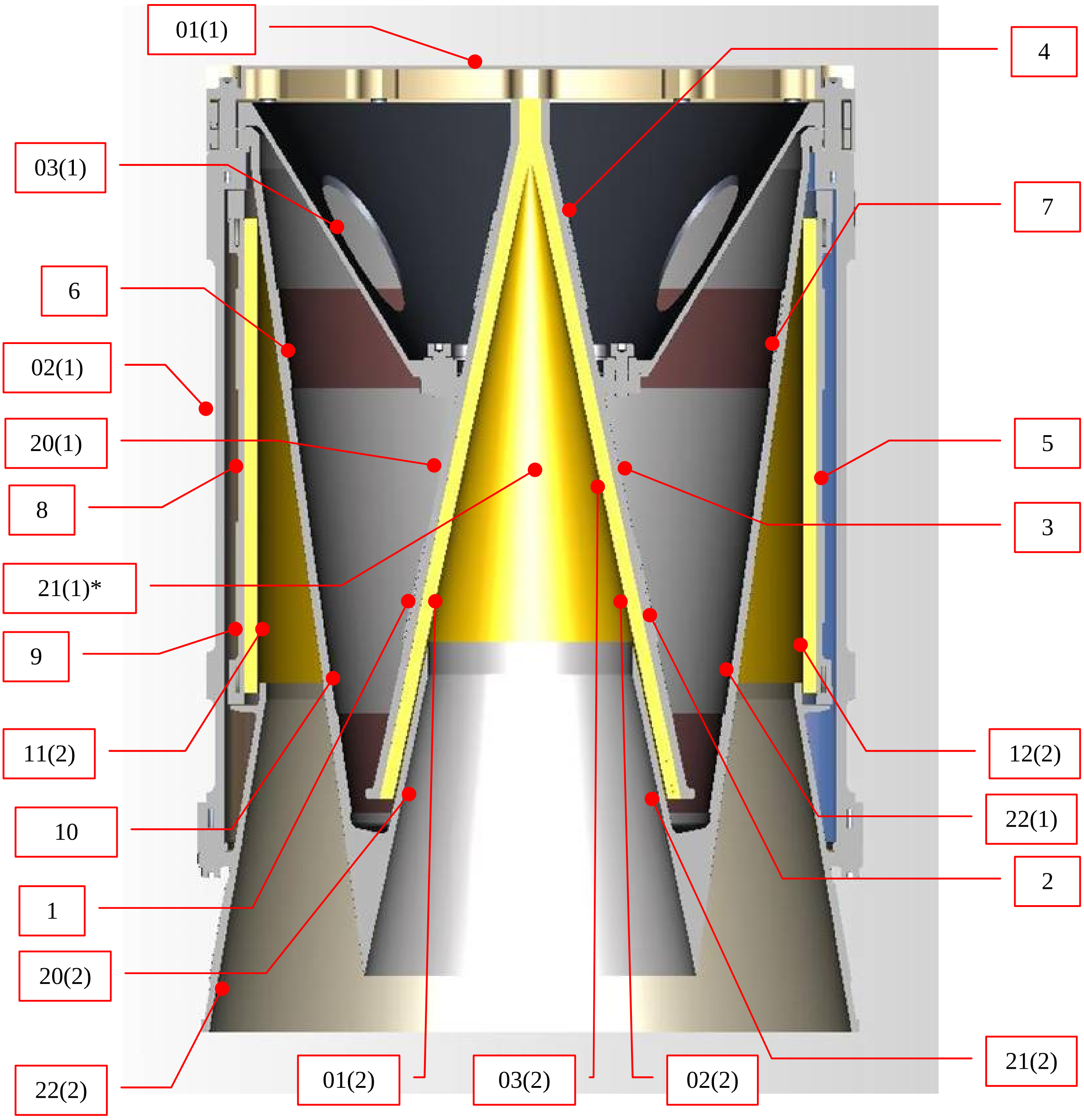

* 21(1) attached to the Secondary Absorber, in the middle.
Note: modification made, but not updated in this figure. Main Absorber was shortened to minimize thermal cross-talk with the Main Reflector - actual overlap is minimal, ~5 mm.

Figure 3-4 HCL temperature sensors locations

Figure 3-5 Diagnostic sensors attached to different surfaces with Kapton and Copper tapes

3.2. Results

The measurements results are summarized in the following tables and graphs (comprehensive results and raw data are stored separately). Time indicated in the table corresponds to the set time of that particular test case interval, at the end of which the thermal equilibrium was reached and data averaged. Normally the averaging is done for 5 minutes of a corresponding test case.

P1 – Main Absorber power
P2 – Secondary Absorber power
P3 – Main Reflector power
P4 – Secondary Reflector power

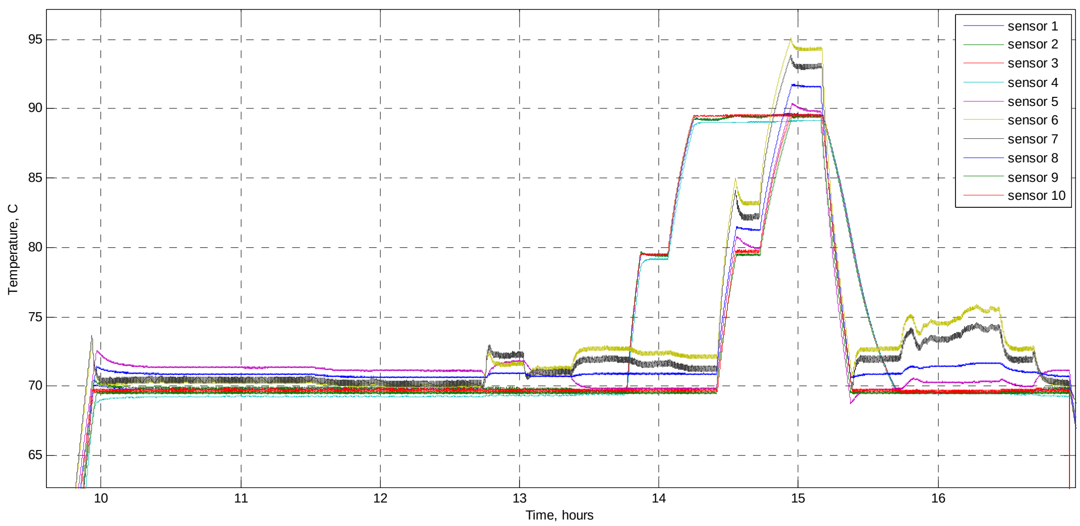

Figure 3-6 Temperature sensors 1-10 data; test cases and time stamps according to Table 3-1 through Table 3-3

Table 3-1

Temp. sensors	0 deg 0m/s T = 70 C t = 12.35	-30 deg 0m/s T = 70 C t = 12.45	30 deg 0m/s T = 70 C t = 13.02	60 deg 0m/s T = 70 C t = 13.22	60 deg 0m/s T = 70 C t = 16.27	0 deg 0m/s T = 70 C t = 16.41
1	69.8	69.8	69.8	69.7	69.7	69.8
2	69.9	69.9	69.8	69.6	69.6	69.9
3	69.6	69.6	69.6	69.6	69.6	69.6
4	69.3	69.4	69.3	69.4	69.4	69.3
5	71.1	71.8	70.7	69.8	70.0	71.1
6	70.1	71.6	71.3	72.8	72.7	70.2
7	70.2	72.3	71.0	72.0	71.9	70.3
8	70.6	71.0	70.7	70.9	71	70.7
9	69.5	69.5	69.5	69.5	69.5	69.5
10	69.7	69.7	69.7	69.7	69.7	69.7
P1	1.9	1.5	2.0	1.8	1.9	1.8
P2	24.6	23.1	22.7	32.7	32.7	27.3
P3	16.3	24.1	22.6	34.0	33.1	17.4
P4	7.5	7.5	7.5	7.5	7.5	7.5
01(1)	49.6	50.8	50.8	51.0	51.1	50.0
02(1)	50.8	50.4	51.3	51.3	49.6	50.4
11(1)	24.9	25.1	25.2	25.3	25.2	25.2
12(1)	25.3	25.5	25.6	25.5	25.3	25.3
20(1)	69.6	69.6	69.6	69.6	69.6	69.6
21(1)	69.7	70.2	69.6	69.1	69.2	69.8
22(1)	69.6	70.2	68.7	68.1	68.1	69.6
03(1)	63.8	64.8	64.8	65.7	65.7	64.2
01(2)	69.0	68.9	68.8	68.3	68.3	68.9
02(2)	68.8	68.8	68.5	66.2	66.2	68.8
11(2)	68.4	66.6	68.6	69.1	69.1	68.4
12(2)	69.1	70.0	66.2	62.4	62.2	69.0
20(2)	68.3	67.5	67.5	66.7	66.7	68.3
21(2)	68.0	68.1	66.3	64.5	64.5	68.0
22(2)	52.0	48.5	51.9	51.1	49.1	51.3
03(2)	69.1	69.1	69.0	68.4	68.3	69.1

Table 3-2

Temp. sensors	60 deg 0m/s T cone = 80 C Tref/abs = 70 C t = 13.46	60 deg 0m/s T cone = 90 C Tref/abs = 70 C t = 14.04	60 deg 0m/s T cone = 90 C Tref/abs = 80 C t = 14.25	60 deg 0m/s T cone = 90 C Tref/abs = 90 C t = 14.45
1	79.4	89.2	89.4	89.6
2	79.4	89.2	89.4	89.5
3	79.5	89.5	89.5	89.6
4	79.2	89.0	89.1	89.2
5	69.8	69.8	80.0	89.8
6	72.4	72.1	83.2	94.3
7	71.6	71.3	82.2	93.1
8	70.9	70.9	81.3	91.6
9	69.5	69.5	79.5	89.4
10	69.7	69.7	79.7	89.5
P1	5.2	9.3	6.6	3.0
P2	32.7	32.7	38.2	46.9
P3	29.3	23.9	35.8	50.5
P4	7.5	7.5	7.5	7.5
01(1)	51.8	52.6	57.2	63.3
02(1)	51.4	51.5	55.7	61.9
11(1)	25.3	25.2	25.2	25.2
12(1)	25.4	25.4	25.4	25.4
20(1)	79.4	89.3	89.4	89.5
21(1)	69.1	69.1	79.0	88.8
22(1)	68.0	67.9	77.7	87.2
03(1)	67.2	68.8	75.7	83.6
01(2)	77.3	86.2	86.9	87.5
02(2)	74.2	82.0	83.2	84.5
11(2)	69	69.0	78.9	88.7
12(2)	62.4	62.5	70.6	78.4
20(2)	67.2	67.6	76.5	85.2
21(2)	64.8	65.2	73.6	81.8
22(2)	51.1	51.1	54.5	59.9
03(2)	77.6	86.9	87.3	87.7

Table 3-3

Temp. sensors	60 deg 1m/s T = 70 C t = 15.52	60 deg 2m/s T = 70 C t = 16.10	RT, no heating t = 08.30
1	69.6	69.5	22.0
2	69.6	69.6	22.0
3	69.6	69.6	21.8
4	69.5	69.5	22.0
5	70.3	70.3	22.2
6	74.7	75.6	22.1
7	73.6	74.2	22.1
8	71.5	71.7	22.2
9	69.5	69.5	22.0
10	69.6	69.6	22.3
P1	2.2	2.0	0
P2	38.3	45.6	0
P3	47.2	52.5	0
P4	7.5	7.5	0
01(1)	50.2	49.1	21.8
02(1)	45.1	42.8	22.0
11(1)	25.3	25.3	22.3
12(1)	25.4	25.3	22.4
20(1)	69.6	69.6	21.8
21(1)	69.3	69.1	21.9
22(1)	67.3	67.1	22.0
03(1)	66.3	66.4	21.9
01(2)	67.2	66.3	21.9
02(2)	66.4	66.2	21.8
11(2)	68.2	68.4	22.0
12(2)	60.9	60.1	22.0
20(2)	65.2	64.1	21.9
21(2)	63.2	63.0	21.8
22(2)	44.3	42.2	21.9
03(2)	67.7	67.3	21.8

3.3. Heaters balancing for the Main Absorber and the Main Reflector.

Results of the tests revealed thermal gradients along the Main Absorber and the Main Reflector. For example a graph below shows reading of the sensors 1-4, located along the Main Absorber, for different tilts.

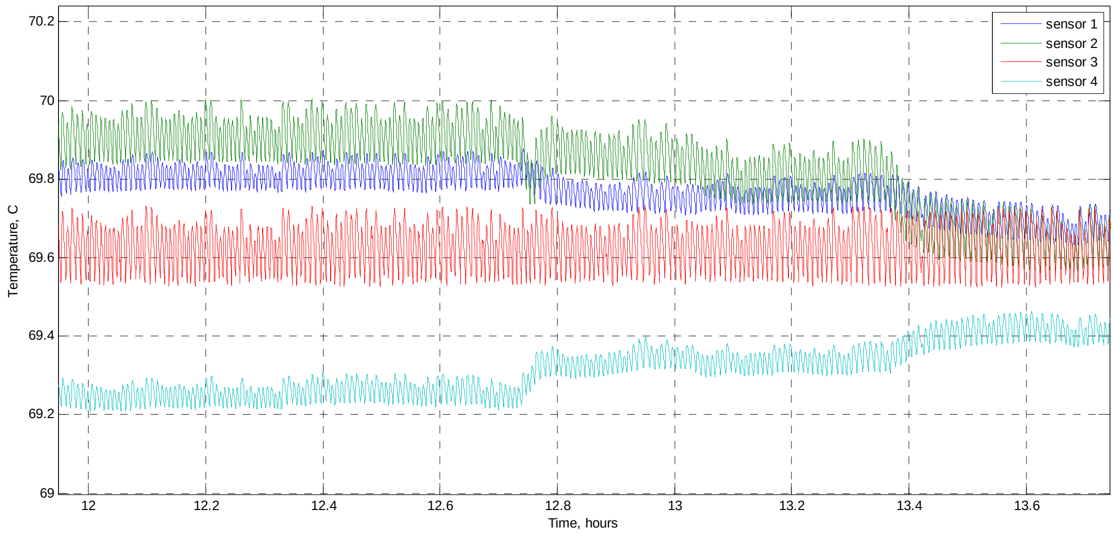

Figure 3-7 Temperature sensors 1-4 data: temperature gradient along the Main Absorber, as a function of tilt, -30÷+60 degrees (test cases and time stamps according to Table 3-1)

These gradients were optimized by balancing power distribution between two parts of each heater circuitry (“top” and “bottom” heaters are connected in parallel) [RD3].
2 heaters patches, out of the original 6, have been removed from the Main Reflector “top” heater.
Also, an extra resistor 43 Ohm has been placed externally in series with the Main Absorber “bottom” heater patches.
Table below shows results of the test after these modifications have been implemented.
Main Reflector gradients are ~3 K now (compared to ~ 5 K before) and that of the Main Absorber is well below 0.3 K (was 0.7 K before), Figure 3-8.

Table 3-4

Temp. sensors	0 deg 0m/s T = 70 C t = 13.16 (day+1)	60 deg 0m/s T = 70 C t = 13.23 (day+1)	60 deg 0m/s T = 70 C Trefl = 80 C t = 14.15 (day+1)
1	69.6	69.5	70.3
2	69.7	69.4	70.2
3	69.6	69.6	70.0
4	69.5	69.6	69.7
5	71.1	69.8	69.7
6	69.2	71.3	80.6
7	69.2	70.0	78.9
8	70.6	70.9	71.1
9	69.5	69.5	69.6
10	69.7	69.6	79.0
P1	2.8	2.8	0
P2	22.9	33.0	21.8
P3	16.9	28.5	50.7
P4	7.5	7.5	7.5
01(1)	49.5	50.8	54.6
02(1)	50.3	50.8	51.7
11(1)	24.0	24.6	24.8
12(1)	24.6	25.0	25.1
20(1)	69.6	69.6	70.2
21(1)	69.7	69.1	69.4
22(1)	69.7	68.2	77.8
03(1)	63.2	64.9	70.6
01(2)	68.9	68.5	69.6
02(2)	68.5	65.9	67.3
11(2)	68.4	69.0	69.6
12(2)	69.0	62.1	62.0
20(2)	68.3	66.7	74.9
21(2)	68.0	64.5	72.2
22(2)	51.7	51.1	52.1
03(2)	69.0	68.6	69.0

Similar to Figure 3-7, this graph shows temperature distribution along the Main Absorber, after power balancing has been applied. The maximum gradients do not exceed 0.3 K.

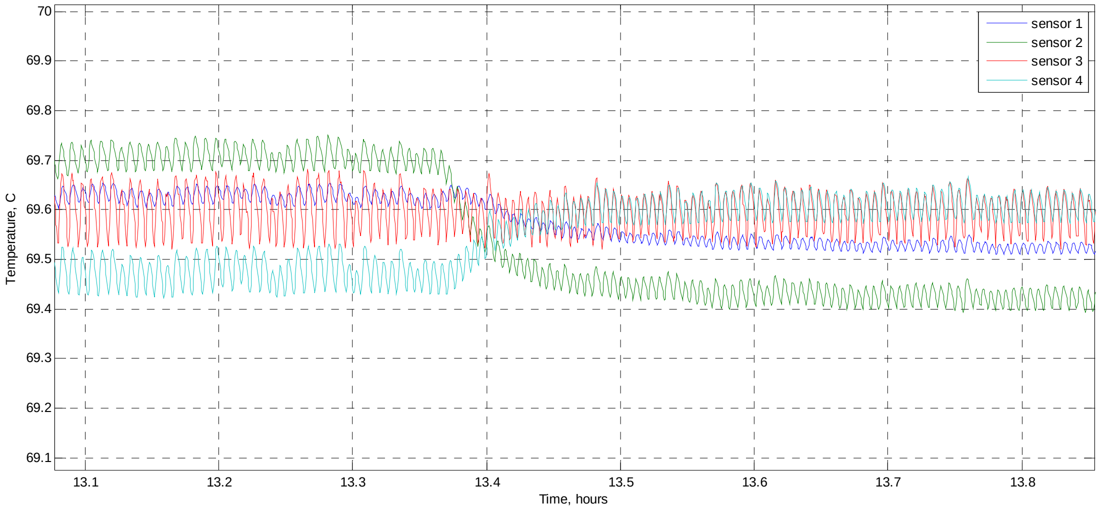

Figure 3-8 Temperature sensors 1-4 data: temperature gradient along the Main Absorber, as a function of tilt, 0÷+60 degrees (test cases and time stamps according to Table 3-4)

3.4. Conclusions

- Thermal performance of the HCL has been tested at different environmental conditions: air flow and tilts. High altitude condition and slightly lower operating temperature in the receiver cabin have not been simulated;
- Heaters for the Main Absorber and Main Reflector have been optimized; thermal gradients as measured on the Main Absorber metal backing do not exceed 0.3 K for a range of tilts between 0 and 60 degrees;
- Surface temperature of absorbers at different locations, and also reflector of the HCL have been measured. However, because temperature sensors do probe temperatures on either side of their mounting, it is likely the readings underestimate the actual physical temperature of the surface;
- High thermal gradients, up to 7 K, are measured on the Secondary Absorber in the cases of large tilt and also airflow. In the case the HCL ought to be used for the Bands 1 and 2, either independent controllers and heaters need to be applied to two halves of that parts, or careful calibrations need to be made;
- Moderate airflow, up to 1 m/s, seems to be tolerable for this design. Still, it is recommended to limit the maximum airflow in the receiver cabin to about 0.5 m/s. Higher airflows do effect performance of the HCL and also increase power consumption;
- HCL reaches thermal equilibrium at 70 degrees set temperature within 30 minutes at lab conditions;
- Power consumption of the HCL is higher than predicted; correlation analysis is on-going;
- MINCO controllers are capable to limit variations in physical temperature of the Main Absorber to within ~0.1 K.

4. INFRARED CAMERA MEASUREMENTS

4.1. Setup

For the infrared measurements we used commercial infrared camera *VarioCAM Research 270* from Jenoptik. The sensor is an uncooled microbolometer of 320x240 pixels. The camera is equipped with a 25mm lens, which gives a field of view of approximately 32x24deg. The angular resolution of the camera is therefore 0.1deg. The camera has been calibrated over several ranges of brightness temperature covering from -40 C to 1200 C. Within the calibrated temperature range, the measurement accuracy specified by the manufacturer is +-2%.

In our measurements, however, absolute accuracy is limited by unknown emissivity of the CR material. Actual emissivity <1 results in underestimation of the derived radiated temperature. On the other side, for specular reflection that are terminated deeper inside of the cone, an emissivity <1 will average out temperature gradients which can persist along or across the cone surface.

4.2. Results

Infrared image of the HCL at 60 degrees tilt is presented in Figure below. A centre circle represents the aperture of the Main Absorber, and the outer ring represents a deep part of the second absorbing cavity (Primary Reflector and Secondary Absorber). An area in between appears to have lower radiation temperature because of its low emissivity and high scatter in infrared (rough Aluminium surface of the Main Reflector).

It is clear that there is thermal gradient in the second absorbing cavity in the plane of the tilt - along vertical cross-section. On the other side, there is no obvious gradient in the same plane for the Main Absorber. Common to all three cross-sections is ~ 2K gradient across the Main Absorber. However, < 1 emissivity of the CR material, in combination with large incidence angle, and also its finite scatter, makes it hard to draw a solid quantitative conclusion about the actual gradient across the load aperture.

Still, one can detect defects in absorbers using this technique. During the manufacturing process of this HCL, a “bulge” (absorber delaminated from the metal backing) appeared in the lower left corner of the Main Absorber (refer to the Figure view), which one can clearly see in the 45 degrees cross-section.

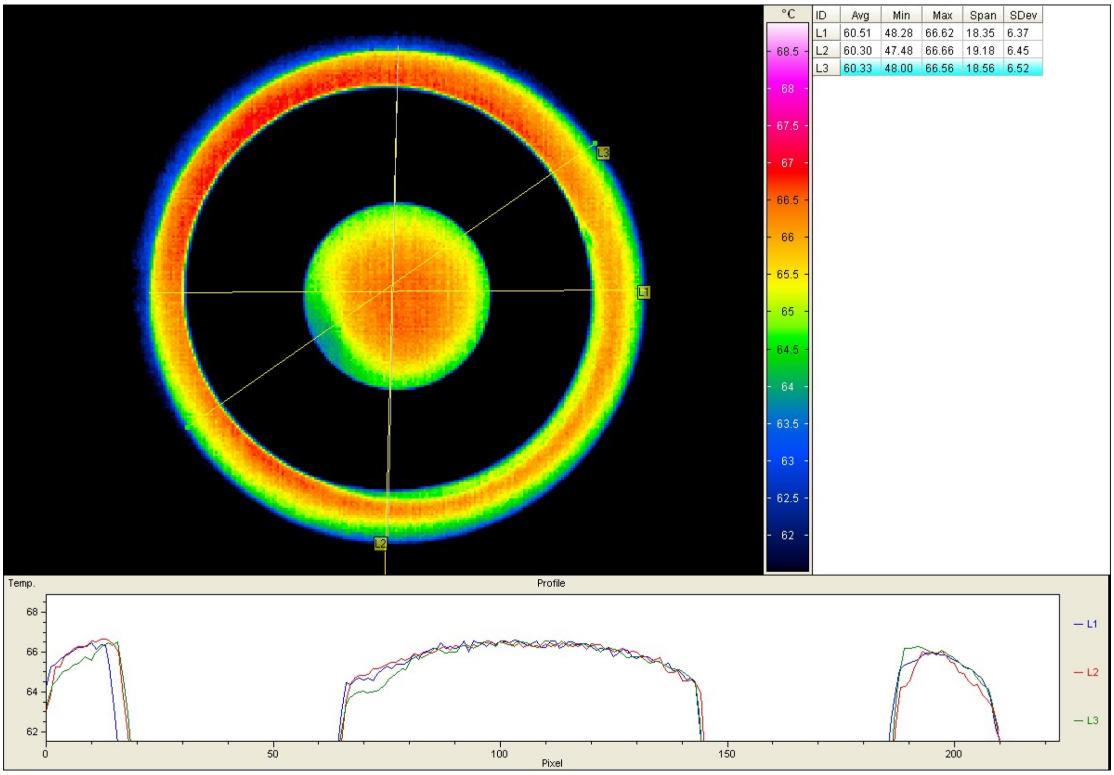

Figure 4-1 Infrared image of the HCL under 60 degrees tilt.
Temperature profiles along three cross sections are presented on the graph below thermal picture.

Figures below show IR images of the production HCL, tested at a nominal temperature of 70C and under 90 degrees tilt. Two Figures below show the central port with the main absorber and the complete HCL aperture, respectively.

The HCL was oriented in a horizontal position to simulate the worst case for convective heatflow. This case has not been tested during the prototype testing, and it will not be present during regular observations with ALMA. The main purpose of this test was to verify that there are no localized cold spots due to delamination or air bubbles in the absorber layer.

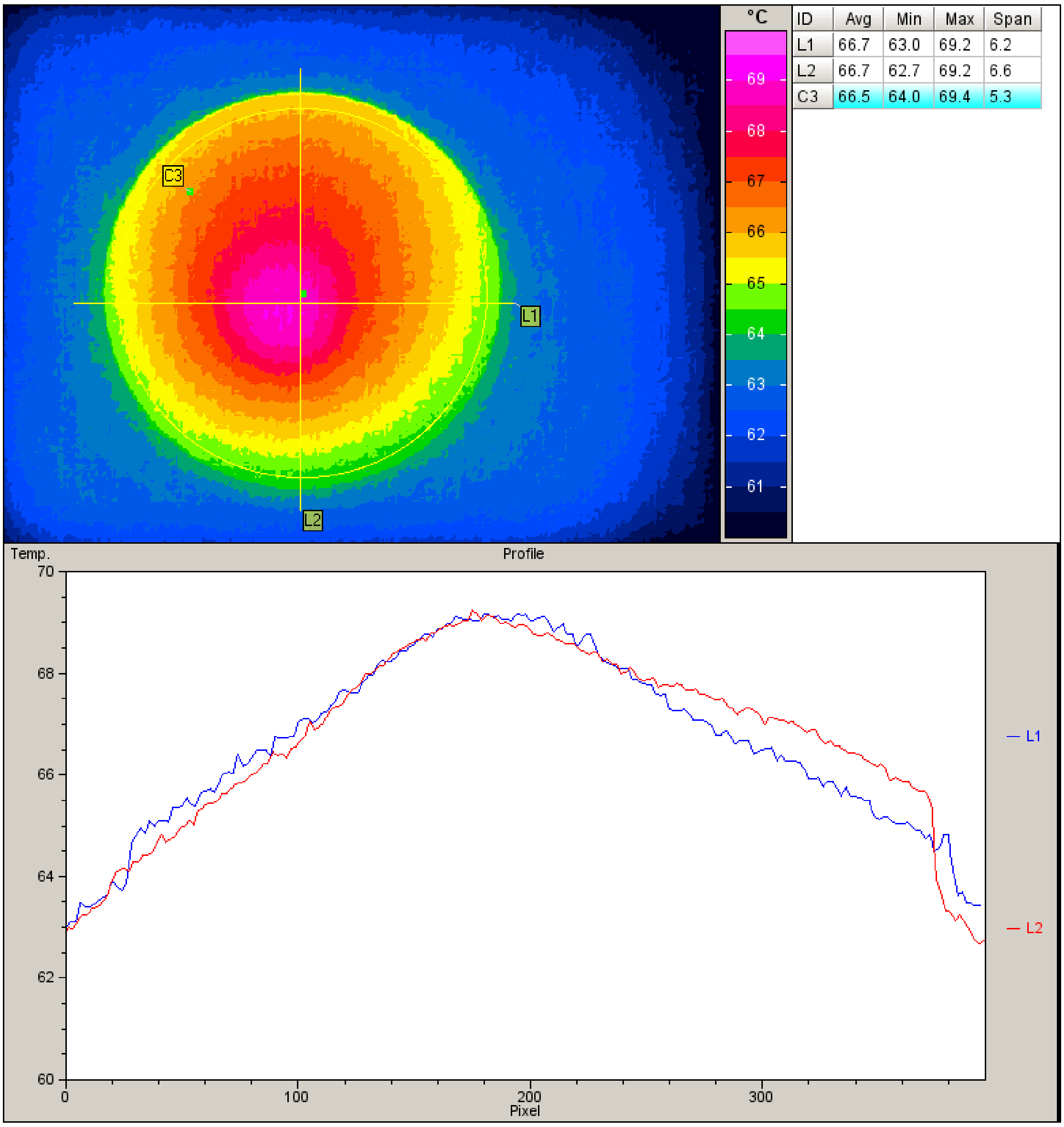

ID	Avg	Min	Max	Span
L1	66.7	63.0	69.2	6.2
L2	66.7	62.7	69.2	6.6
C3	66.5	64.0	69.4	5.3

Figure 4-2 IR image of the main absorber cone.
Besides the expected gradient from the convection no sign of delamination has been found.

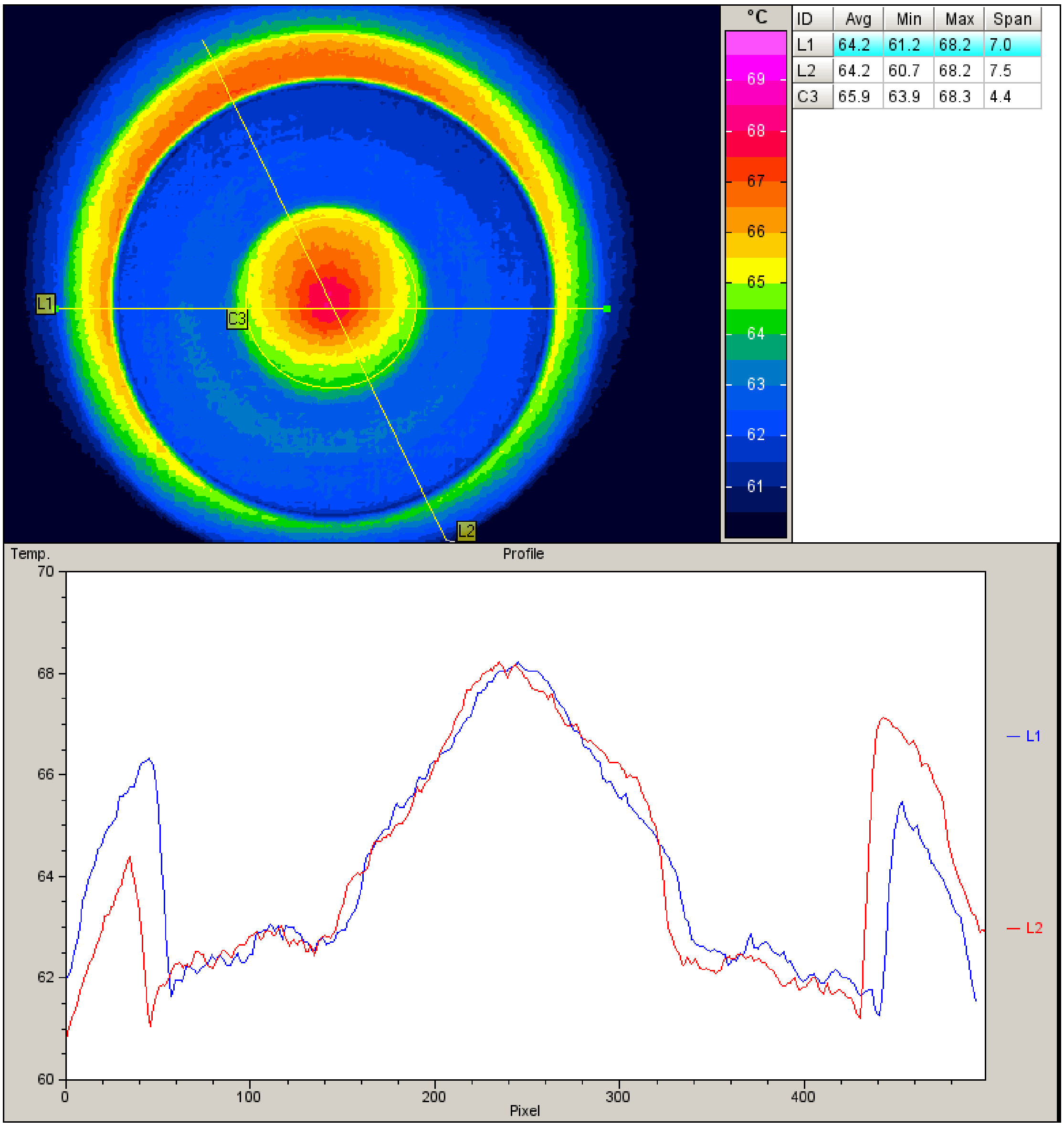

ID	Avg	Min	Max	Span
L1	64.2	61.2	68.2	7.0
L2	64.2	60.7	68.2	7.5
C3	65.9	63.9	68.3	4.4

Figure 4-3 IR image of the complete target aperture.
The gradients on the secondary absorber are significantly larger than in the main absorber, which is expected from the thermal simulations.

5. RADIOMETRIC PERFORMANCE

5.1. Radiometric performance @ 91 GHz

The radiometric performance of the HCL has been investigated with a 91GHz radiometer. This instrument operates in two orthogonal polarizations with 2GHz bandwidth. It is equipped with uncooled W-band preamplifiers (RPG, NF 4-5dB) and single sideband filters. For the internal calibration the signals of two noise diodes can be injected through directional couplers. For the external calibration a switching mirror is inserted in front of the corrugated feed horn by a magnetic actuator. For the radiometric tests the HCL was mounted in a vertical position above this switching mirror and the ACL directly in front of the feed (see Figure 5-1).

The calibration sequence consisted of the 4 cycles, each of about 4s, during which the total power coming from the radiometer was recorded while observing on the HCL and ACL with and without injecting noise from the noise diode. By checking that ratio of the differences between HCL and ACL measurements with and without noise diode is close to unity we were able to verify that our measurement accuracy is not degraded by nonlinearities.

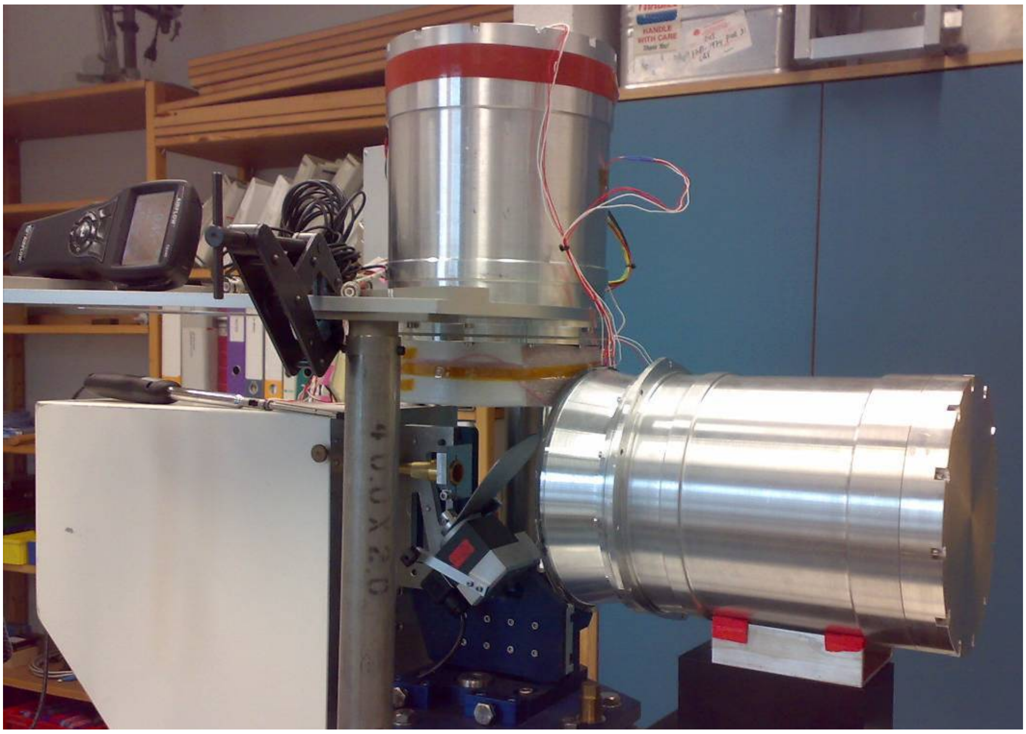

Figure 5-1 Radiometric test setup with ACL and HCL in front of the 91GHz receiver.

The amplitude of the noise diodes was calibrated before, in the middle and at the end of the test series using a “dripping” LN2 cold load made of pyramidal foam absorber. The physical temperature of the ACL and HCL was recorded during the whole test sequence using the ACD temperature controller. The apparent radiometric brightness temperature of the HCL was then determine at different set temperatures of 70, 80 and 90 C by a total power calibration based on the ACL reading with and without noise diode. This calibration assumes that the ACL and the LN2 target are perfect blackbody targets. Any bias on their apparent brightness temperatures will lead also to a wrong estimate of the HCL brightness temperature.

Figure 5-2 shows the complete time series of the radiometric tests at the three set temperatures. It compares the calibrated radiometric HCL temperature (red circles) with the readings of the following HCL temperature sensors:
“cone” - Main Absorber, sensor 20(1);
“cylinder” – Secondary Absorber, sensor 21(1);
“reflector” – Main Reflector, sensor 22(1)
Sensors may be referred to Figure 3-4 in previous section. The optical beam is coupled into Main Absorber, so “cone” reading represents physical temperature of the absorber.

Between 13.35 and 13.45 hours the commercial fan “ELTA” was used to simulate a forced airflow of about 1 m/s. The zoom on that set temperature in Figure 5-3 shows that the forced airflow resulted in a suppression of the radiometric HCL temperature of about 0.5 K.

The average bias between the radiometric HCL temperature and the reading of the HCL “cone” sensor without forced airflow is summarized in the following table. Two different sets of biases are presented. For the first one the mean value of three LN2 calibration cycles of the noise diode temperature has been used, which results in a rather small HCL bias of <-0.3K which remains almost constant for the different set temperatures. The same calibration has been applied to the results in Figures 5-3 to5-6.
Each LN2 calibration led to slightly different values of the noise temperature, however. If we trust only the last LN2 calibration the resulting bias is twice as high and increases as expected with the set temperature.

Bias	70 C	80 C	90 C	calibration of noise diode temperature
ΔT [K]	-0.24	-0.30	-0.29	mean of three LN2 calibrations at t = 13.3, 14.7 and 15. 4
ΔT [K]	-0.54	-0.66	-0.71	only one LN2 calibration at 15.4 used

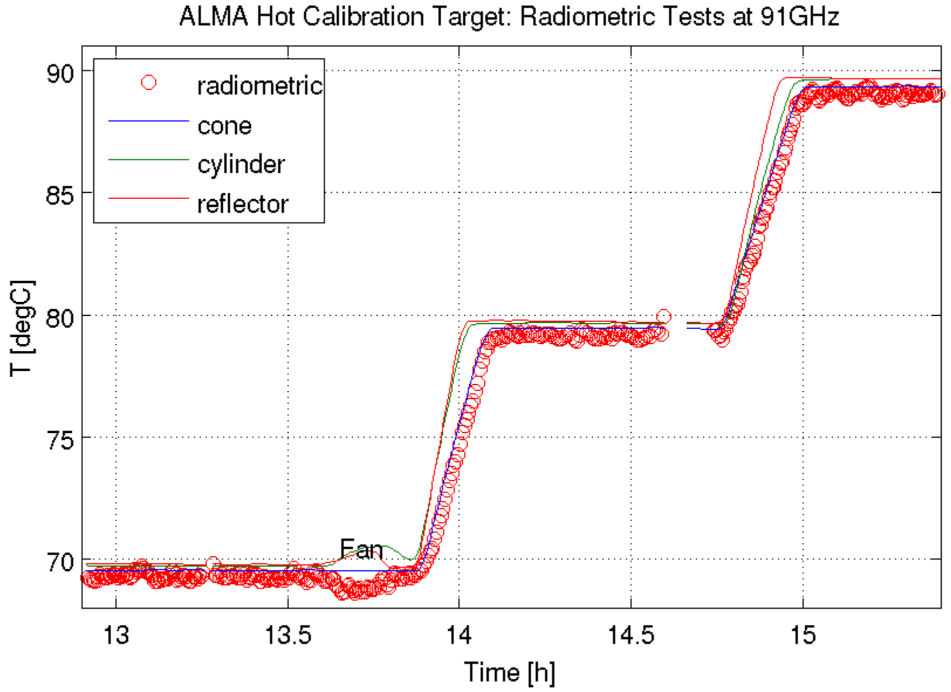

Figure 5-2 Complete time series of the radiometric tests at three different set temperatures.

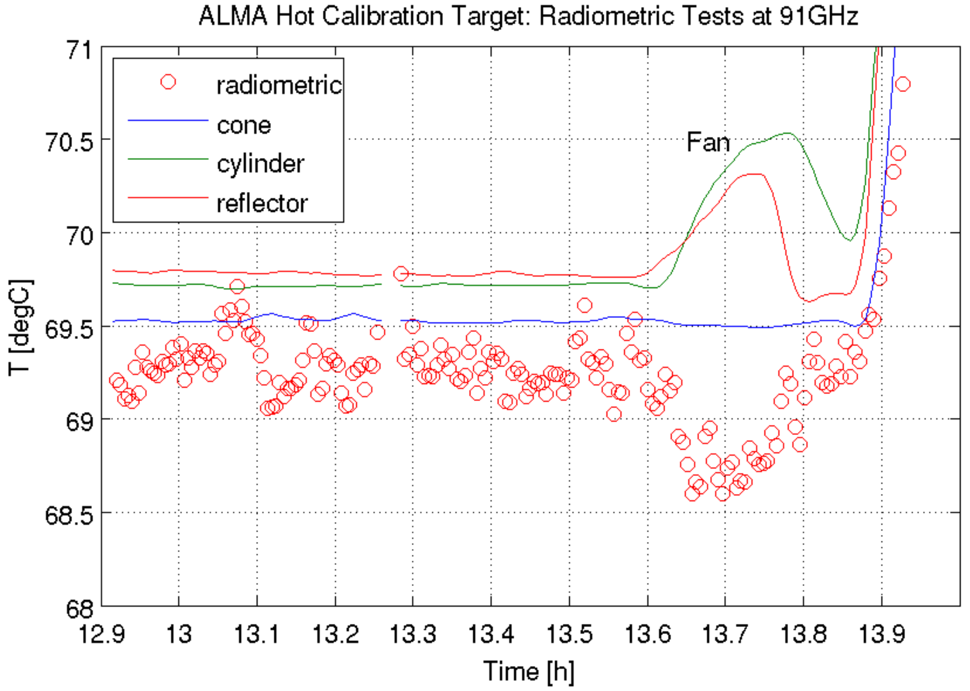

Figure 5-3 Radiometric temperature and HCL sensor readings at 70C set point temperature. Between times 13.6 and 13.8 a forced air flow of about 1m/s was introduced with a fan.

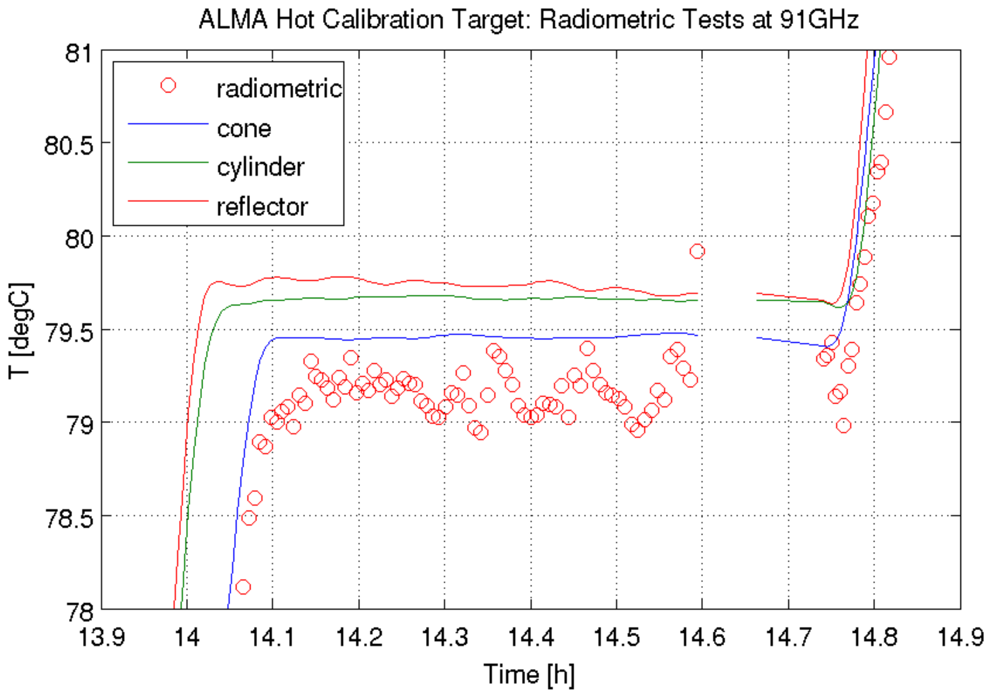

Figure 5-4 Radiometric temperature and HCL sensor readings at 80C set point temperature.

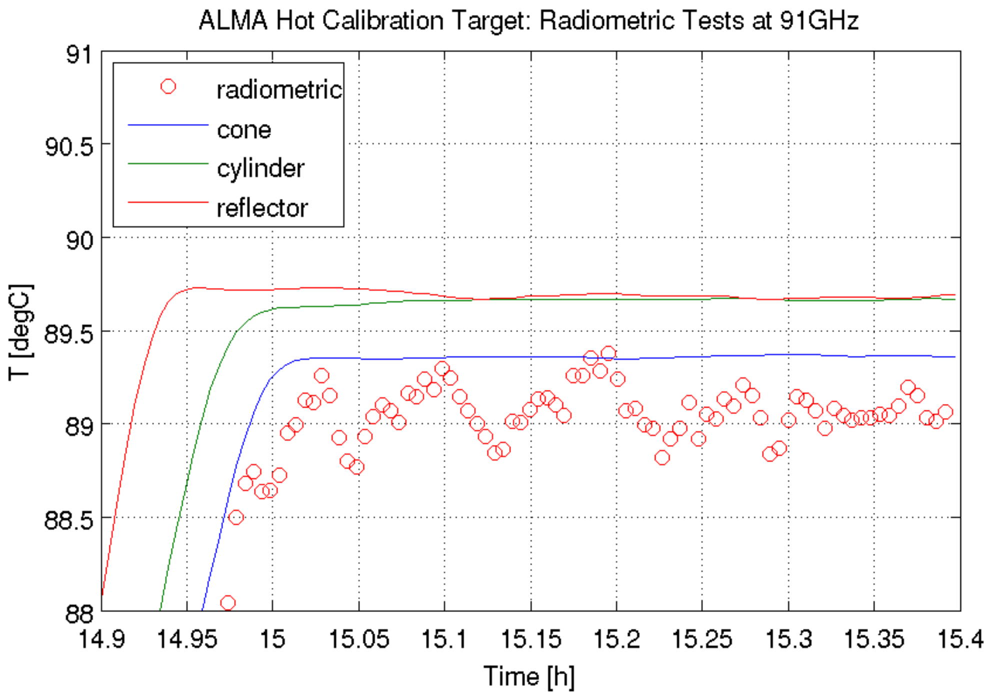

Figure 5-5 Radiometric temperature and HCL sensor readings at 90C set point temperature.

5.2. Radiometric performance @ 700 GHz

Radiometric performance of the Loads has been investigated at 700 GHz using ALMA Band 9 receiver. The measurements were done at SRON using one of the production cartridges. Test setup consists of the ALMA Band 9 receiver and three Calibration Loads:

Hot Calibration load (HCL)
Ambient Calibration Load (ACL)
Cold Calibration Load (CCL).

The HCL and ACL are prototype ALMA Calibration Loads, as presented at the ACD CDR in December 2009. The CCL is a LN2 target normally used by the Band 9 group for the receiver noise tests. It consists of a metal basket, filled with liquid nitrogen. Inner walls of the basket are coated with ~1 mm SiC coating. Optical beam is directed to the basket by means of the two Aluminum mirrors, both at room temperature.
A procedure to derive an unknown temperature of one of the three loads assumes that one knows accurately the effective temperatures of the two other loads and that that the system is linear.

Calibration Loads temperature uncertainty
There is quite some uncertainty in the effective temperature of the CCL due to reflection at the liquid nitrogen surface, <1 emissivity of SiC coating, absorption in atmosphere, resistive loss in the metal mirrors, and their spillover.
Only reflection loss at the LN2 surface contributes to ~1.5-2K extra, so adding emissivity and atmospheric contribution it is safe to assume an effective temperature of the load to be >80K.
An error in the CCL transfers to the error in the derived HCL with a gain factor (Th-Ta)/(Ta-Tc) = 0.2÷0.3 in the Th range 70÷90C. In other words, underestimating the CCL with 1K results in overestimating the HCL by 0.2÷0.3K in this temperature range.
All above mentioned sources of uncertainties do not apply to the ACL. The only potential error could be due to the temperature sensor accuracy, which has been taken care of by a careful calibration. So we are confident that the ACL effective temperature is accurate to <±0.2 K and this translates one to one into the HCL error budget.

System linearity
Non-linear response of the receiver, including the read-out electronics, contributes to the measurements accuracy. Very careful characterization of the system has been made, including optimization of all receiver operating parameters (LO frequency, power, SIS bias). After all, the remaining *small signal* non-linearity of the system was measured to be 0.4% between the 80K and 373K backgrounds. See details of the measurement technique in the corresponding Band 9 Test Procedures document. This measured small signal compression translates into 0.2% large signal compression and our estimates show (not included here) that this effect contributes to 0.15K underestimation in the derived HCL effective temperature. No correction for this effect was made in the results presented below.

Results of the measurements are presented in Table 1 and Figure 5-6 below. Both polarization of the receiver were recorded. Pol0 has a receiver noise Trx=110K, Pol1 Trx=135K.

Table 1. HCL set temperatures and derived effective temperatures. 'MA' stands for Main Absorber, 'SA' for Secondary Absorber, and 'MR' for Main Reflector. In the case of Band 9 most of the beam is confined within the MA, so its physical temperature mostly determines the effective temperature of the load.

T, C	MA	SA	MR	HCL from Pol0 channel Tc=80K	HCL from Pol1 channel Tc=80K	HCL from Pol0 channel Tc=84K	HCL from Pol1 channel Tc=82K
70	70	70	70	70.6	70.4	69.8	70.1
80	80	70	70	81.2	80.2	80.3	79.8
86	86	80	80	87.3	86.1	86.3	85.7
90	90	80	80	91.6	90.8	90.5	90.3

First we assumed the CCL temperature, Tc, to be 80 K. One can see rather good correlation with the set temperatures 70, 80, 86 and 90 C. However, there is obviously a systematic deviation of the derived temperature of ~1K in the case of Pol0 and ~0.5K in Pol1, getting larger at higher temperatures. This indicates that there is likely to be an error in determining the receiver gain from the CCL and ACL measurements. As discussed above, our estimate of the CCL temperature, 80K, does take into account reflection at the liquid nitrogen surface and final emissivity of the SiC absorber, but not losses in the two RT mirrors and their spillover. Applying corrections to the cold load temperature of 4K and 2K for Pol 0 and Pol 1, respectively, brings the estimated and set temperatures much closer to each other. One should notice that this 1-2 K noise contribution from each mirror due to spillover and resistive loss is not at all unrealistic and in line with our previous experience. Also, it is not likely that the effective temperature of the HCL would be larger than the physical temperature of the MA, although the latter is measured at the metal backing of the cone. Most importantly is to note that it is extremely unlikely that the CCL is >90K, in which case the derived HCL effective temperature would reach a 1K offset in temperatures, a limit set by the technical specifications.

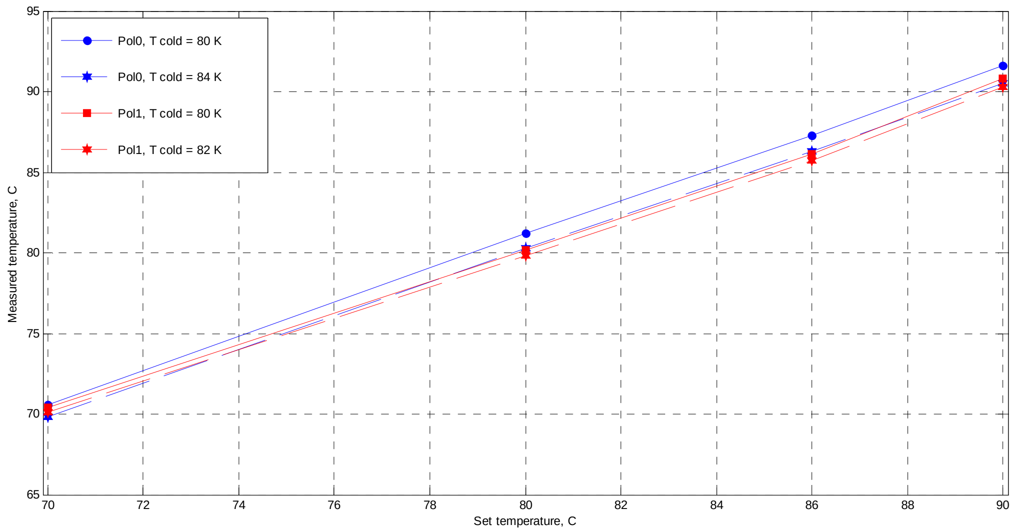

Figure 5-6. Derived effective temperatures of the HCL vs. set temperature. Solid lines assume the cold load temperature 80 K, and dotted lines assume Tc 82K and 84K.

Acknowledgments.
Band 9 team is greatly acknowledged, especially technical support from Jan Barkhof.

5.3. Effective temperature of the Loads as a function of tilt

Performance of the ALMA Calibration Loads effective temperature as a function of tilt has been verified at the European Front End Integration Center using Band 3 and Band 9 receivers. The Loads were attached to the FESS in front of the ALMA cryostat, as shown in the Figure 5-7 below. Original idea was to place both loads on the beam scanner and be able to alter those automatically during the tilt test. However, due to late beam scanner delivery the system was not ready, so we had to use a soft Eccosorb for calibrations for both cold load (LN2 cooled) and also ambient load. This has created rather large uncertainly in the effective temperature of the ambient load, because of its poor backscatter performance and thus reproducibility and also temperature variations in the room due to HVAC system. Problem with temperature variations are clearly seen in Figure 5-8.

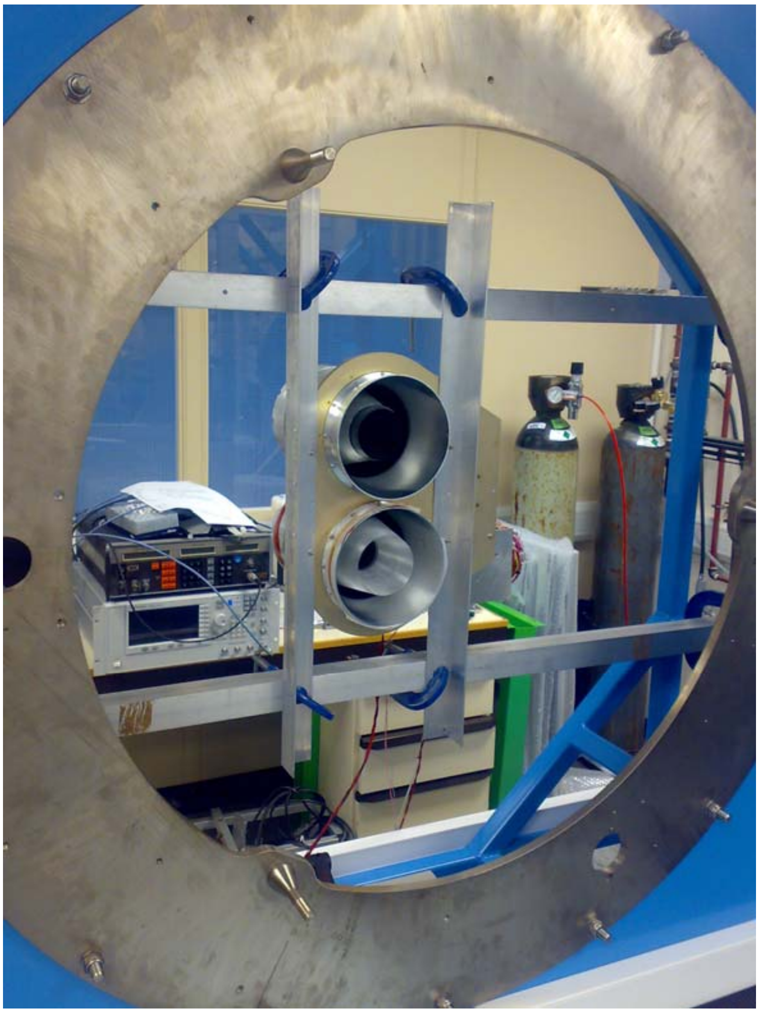

Figure 5-7. ALMA prototype Calibration Loads installed on the FESS. Only one load can be used at a time, so that a piece of soft Eccosorb was used for either cold (liquid nitrogen) or ambient calibrations.

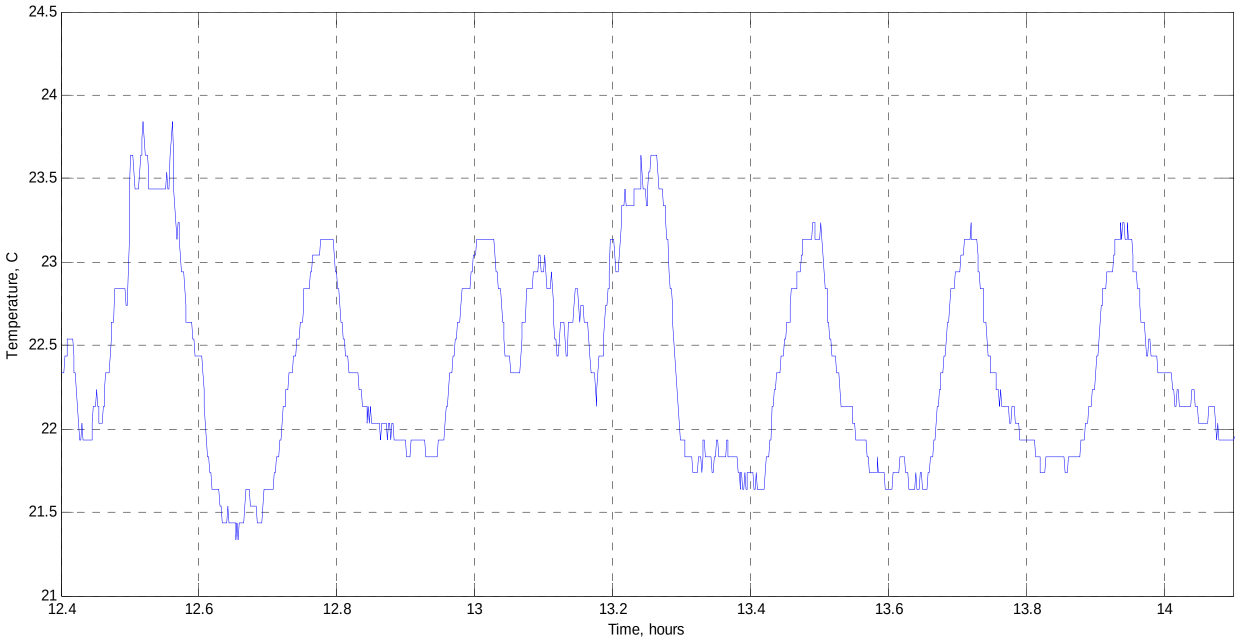

Figure 5-8. Temperature variations in the room. Temperature sensor is located close to the cryostat top lead. Between 13 and 13.30 tilt test was done.

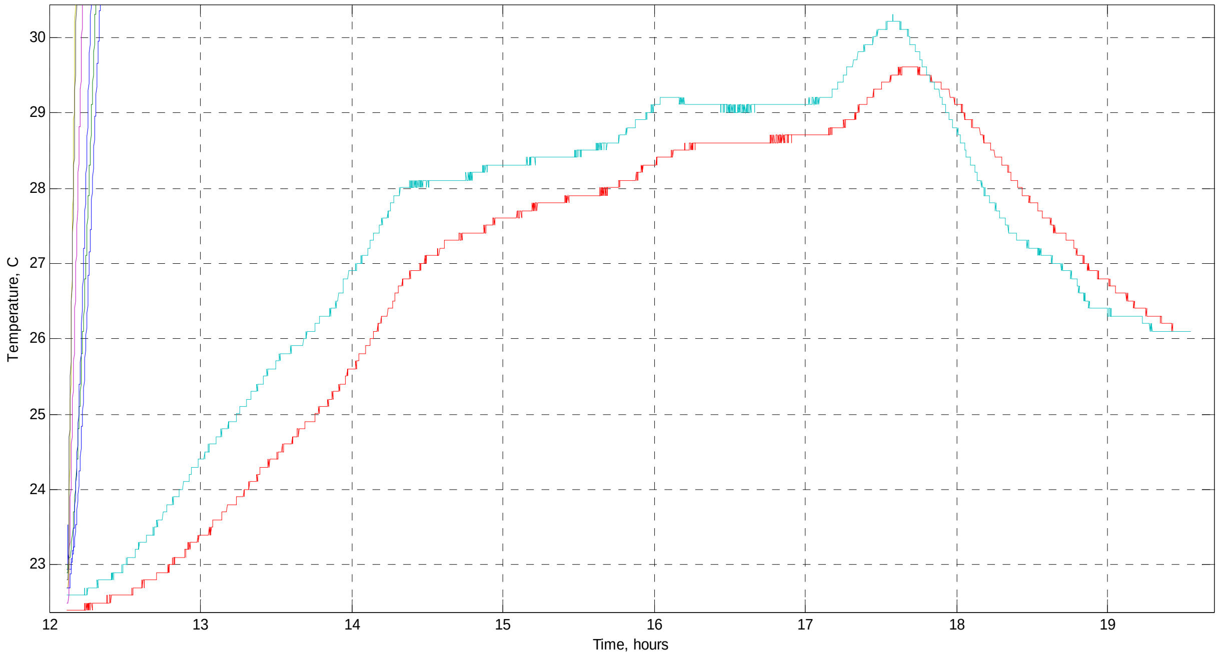

Figure 5-9. ALMA Ambient Calibration Load temperature, one sensor attached to the Main Absorber, and the other to the Secondary Absorber.

For comparison, Figure 5-9 shows physical temperature of the ACL, which does not show fast variations, due to its good thermal isolation and also large thermal capacity. ACL has slightly higher than the ambient temperature due to thermal coupling to the HCL via common mounting plate and convection. Thermal isolation between the loads will be further improved for the production units.
The tests performed *only* aimed at the effective temperature *variation* as a function of tilt. Thus no calibration of the receiver linearity or read-out system dynamic range was done.
The main contribution to the error budget in these measurements is variation in the ambient load temperature. These variations translate approximately one-to-one tot the derived effective temperature of the HCL, see Figure 5-10.

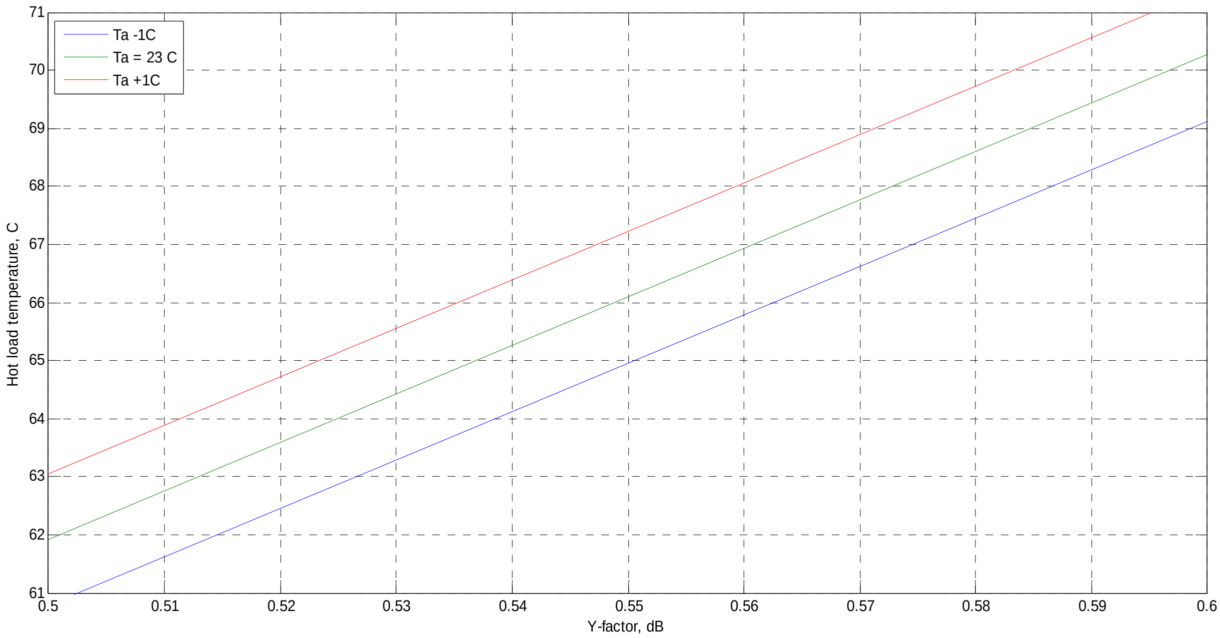

Figure 5-10. Derived HCL effective temperature from the measured Y-factor (Hot Load-Ambient Load). Also shown sensitivity to the ±1C uncertainties in the ambient load temperature.

Another uncertainty is variation in the receiver noise temperature. This variation can in principle be calibrated out by using three loads. However, the hand-hold nitrogen cooled load was found to be not reproducible, see below, so that we have decided to rely on stability of the receiver noise temperature and thus dP/dT vs. tilt. Also, the derived HCL temperature is not very critical to this variation, especially in the case of low receiver noise, see Figures 5-11 and 5-12.

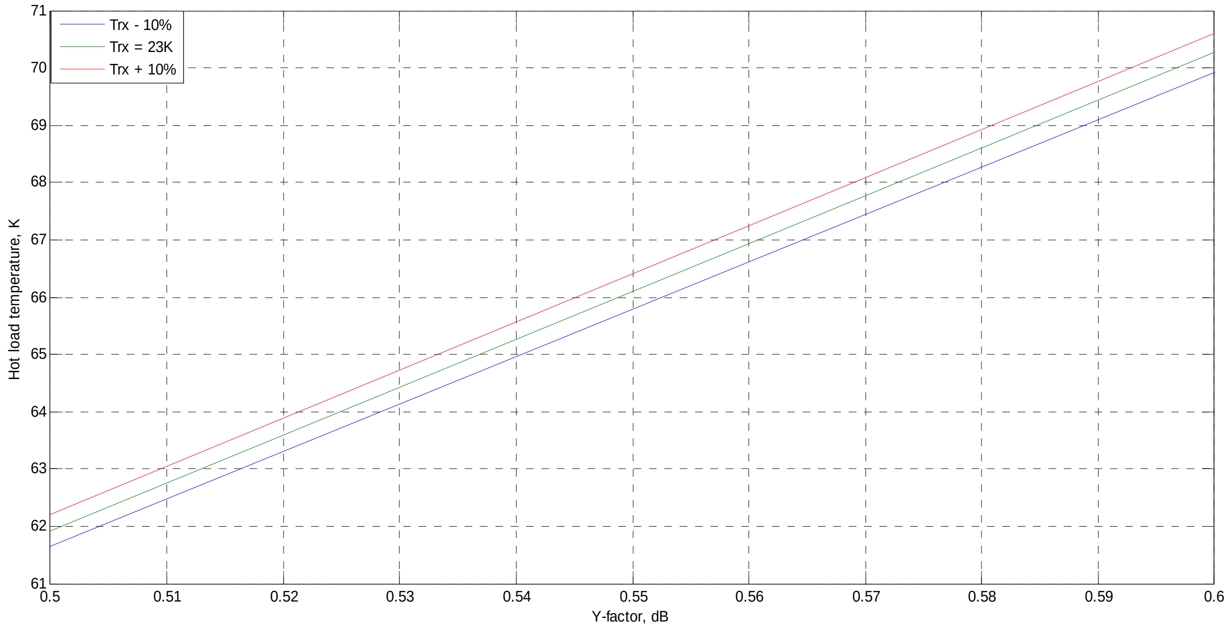

Figure 5-11. Derived HCL effective temperature from the measured Y-factor (Hot Load-Ambient Load (23C)). Also shown sensitivity to the ±10% variations in the receiver noise temperature around Trx = 23K.

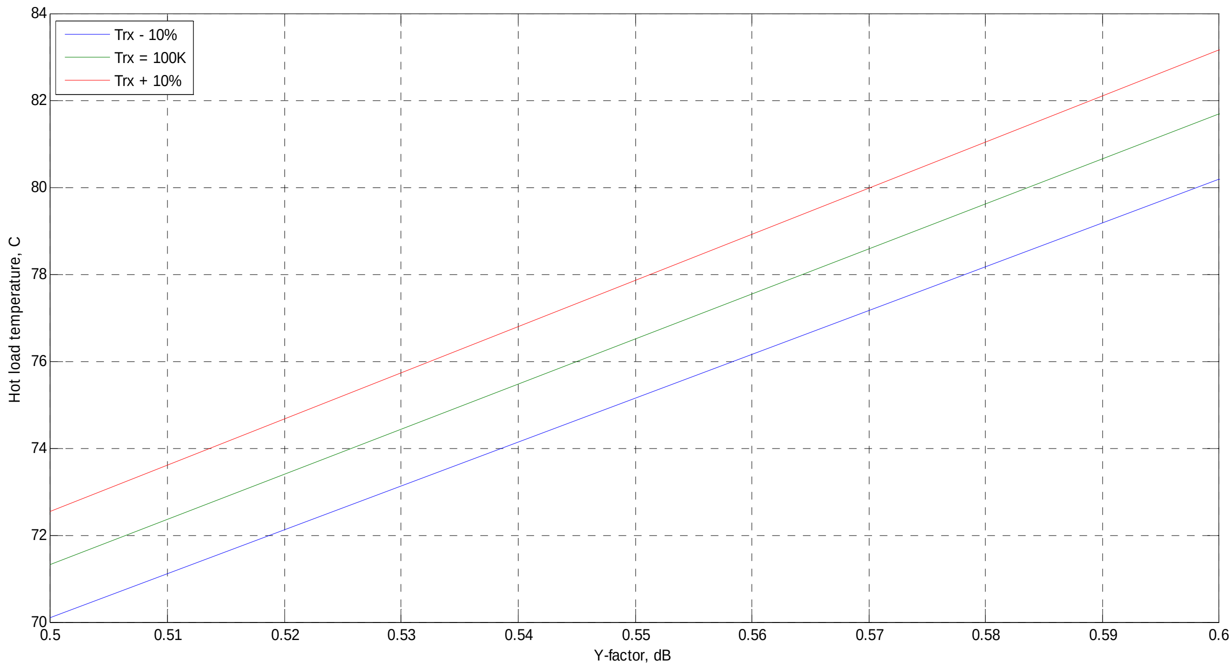

Figure 5-12. Derived HCL effective temperature from the measured Y-factor (Hot Load-Ambient Load (23C)). Also shown sensitivity to the ±10% variations in the receiver noise temperature around Trx = 100K.

Test 1.

Measurements with Band 3 started around 13.00 (RT sensor data in Figure 5-8 correspond to that period) and last for 30 minutes. During this test the dewar was tilted 0-30-60-90 degrees in three steps and then returned to 0 degrees in one move. Recorded IF power levels are shown in Figure 5-13. One can easily see times periods when the tilt table moved, around 3, 6, 11 and 22 minutes. Two calibrations with cold load were done around 17-18 minute, that time the dewar was at 90 degrees tilt. A dedicated algorithm was developed to process the data and finally derive the Y-factor, lower panels of this Figure 5-13 indicate this process. One can see a drift in the beginning of the measurements, at the time the dewar was still at 0 degree position. It's likely that the ambient load got a bit warmer in the beginning of the tests due to vicinity of the hot load, thus reducing the Y-factor. Also, temperature in the room was on a positive sloop, see Figure 5-8, can also explain that trend. Besides that, there is no sign of variation in the measured Y-factor as a function of tilt, also when the dewar returned back to 0 degree position. Note that 1 K variation in the load temperature corresponds to approximately 0.01 dB variation in the measured Y-factor.

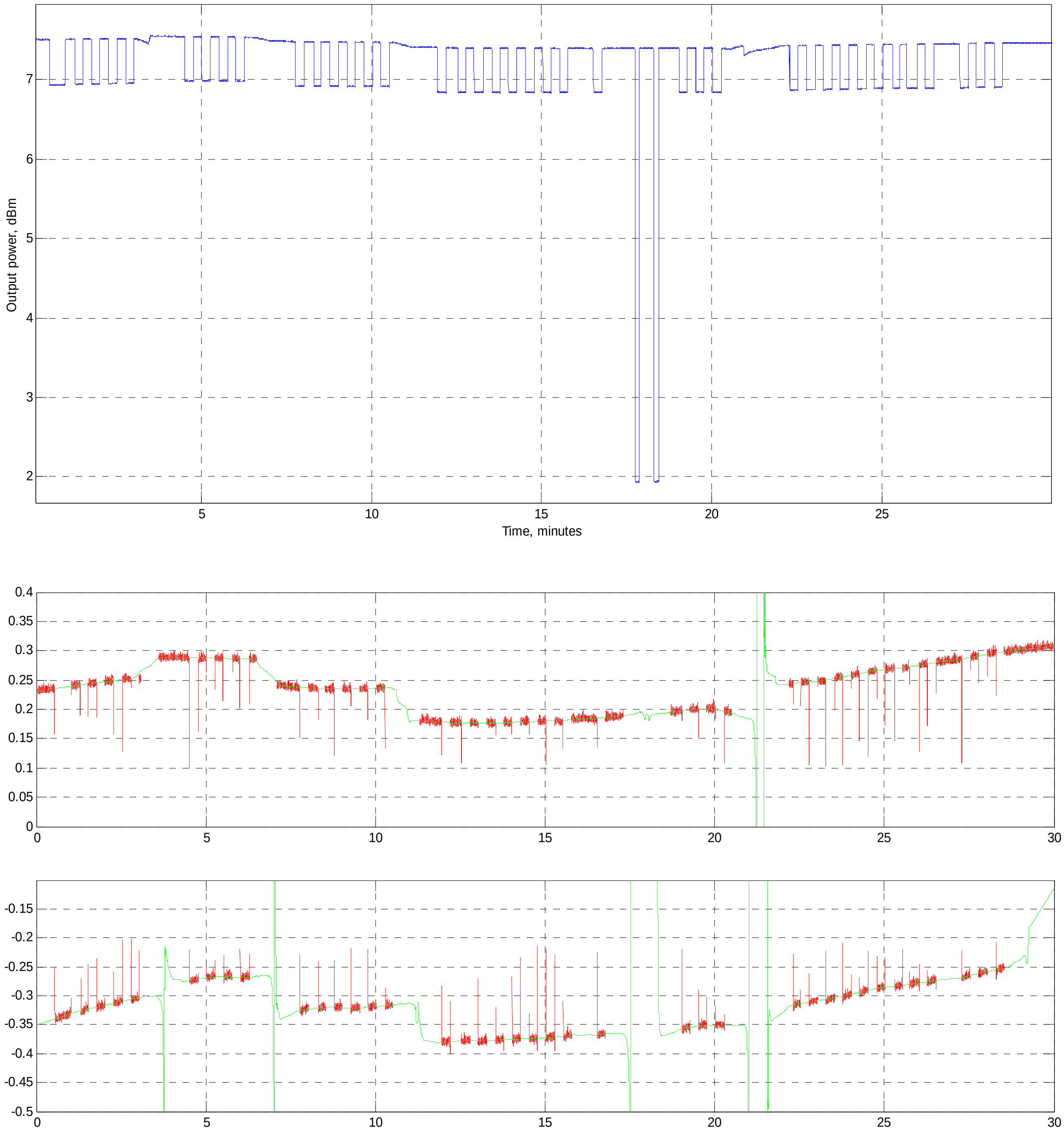

Figure 5-13. Band 3 test. Upper panel – IF output power for three loads: ALMA HCL, hand-held flexible Eccosorb at ambient (~23C) and LN2 cooled. Tilt table moved 0-30-60-90-0 degrees, around 3, 6, 11 and 22 minutes. Lower panels just show how the data was processed: hot load in the upper panel and ambient in the lower. Discontinuities in the smoothed curves will not be considered, see Figure 5-14.

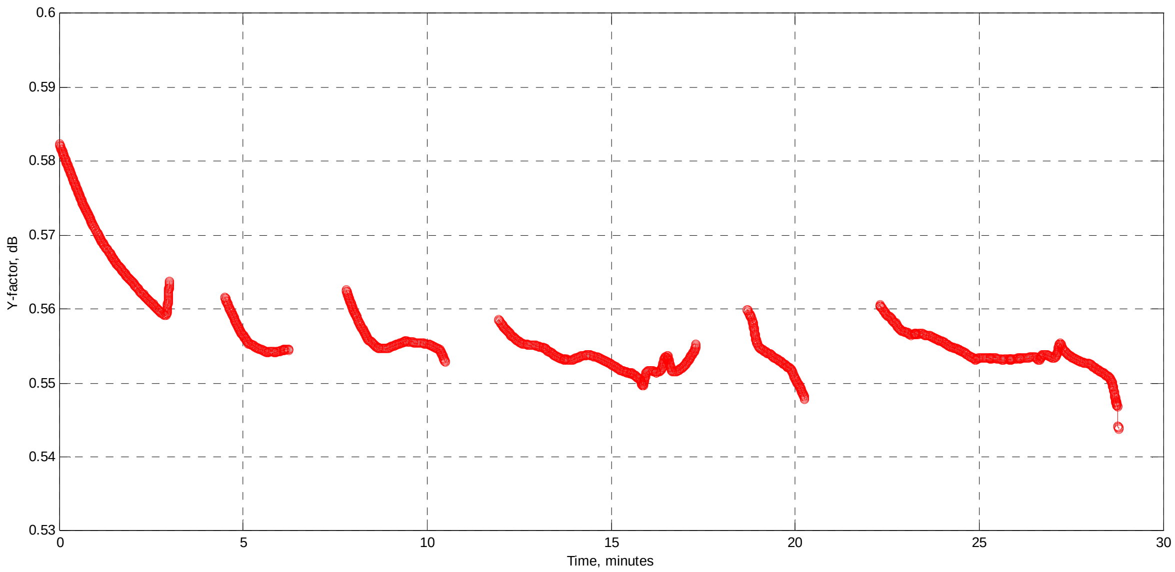

Figure 5-14. Y-factor derived from Hot-Ambient measurements. It's likely that the ambient load got a bit warmer in the beginning of the tests due to vicinity of the hot load, thus reducing the Y-factor. Also, temperature in the room was on a positive sloop, see Figure 5-8, can also explain that trend. Besides that, there is no sign of variation in the measured Y-factor as a function of tilt, also when the dewar returned back to 0 degree position.

Test 2.

Band 9 receiver was used to measure loads performance with 10 degrees steps. At each step three calibration loads were used. Results are presented in Figure 5-15.

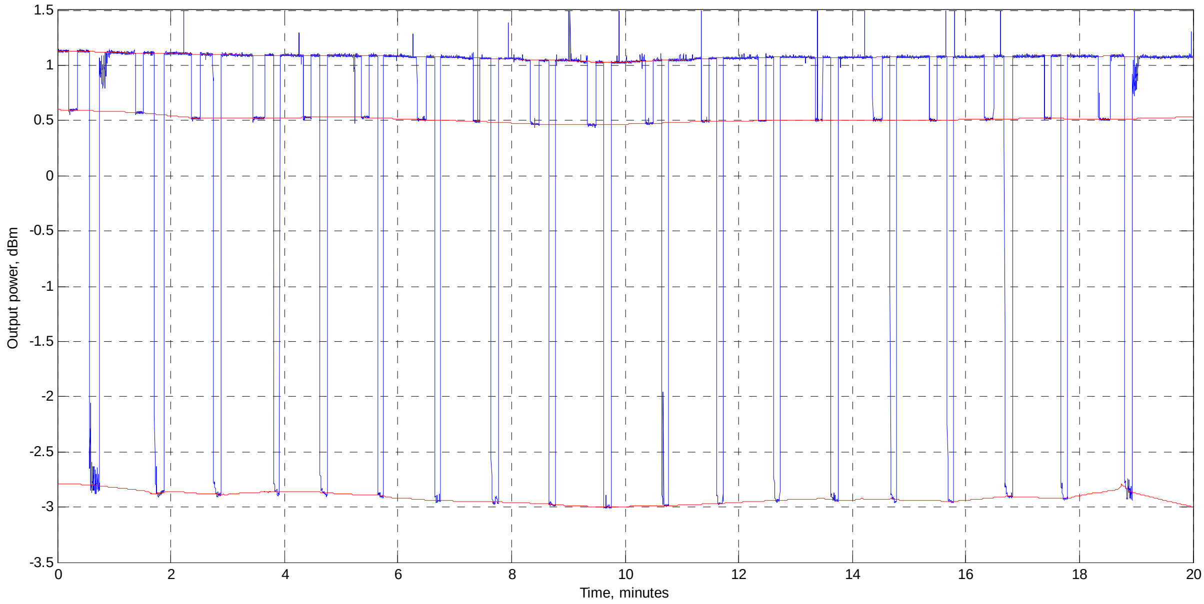

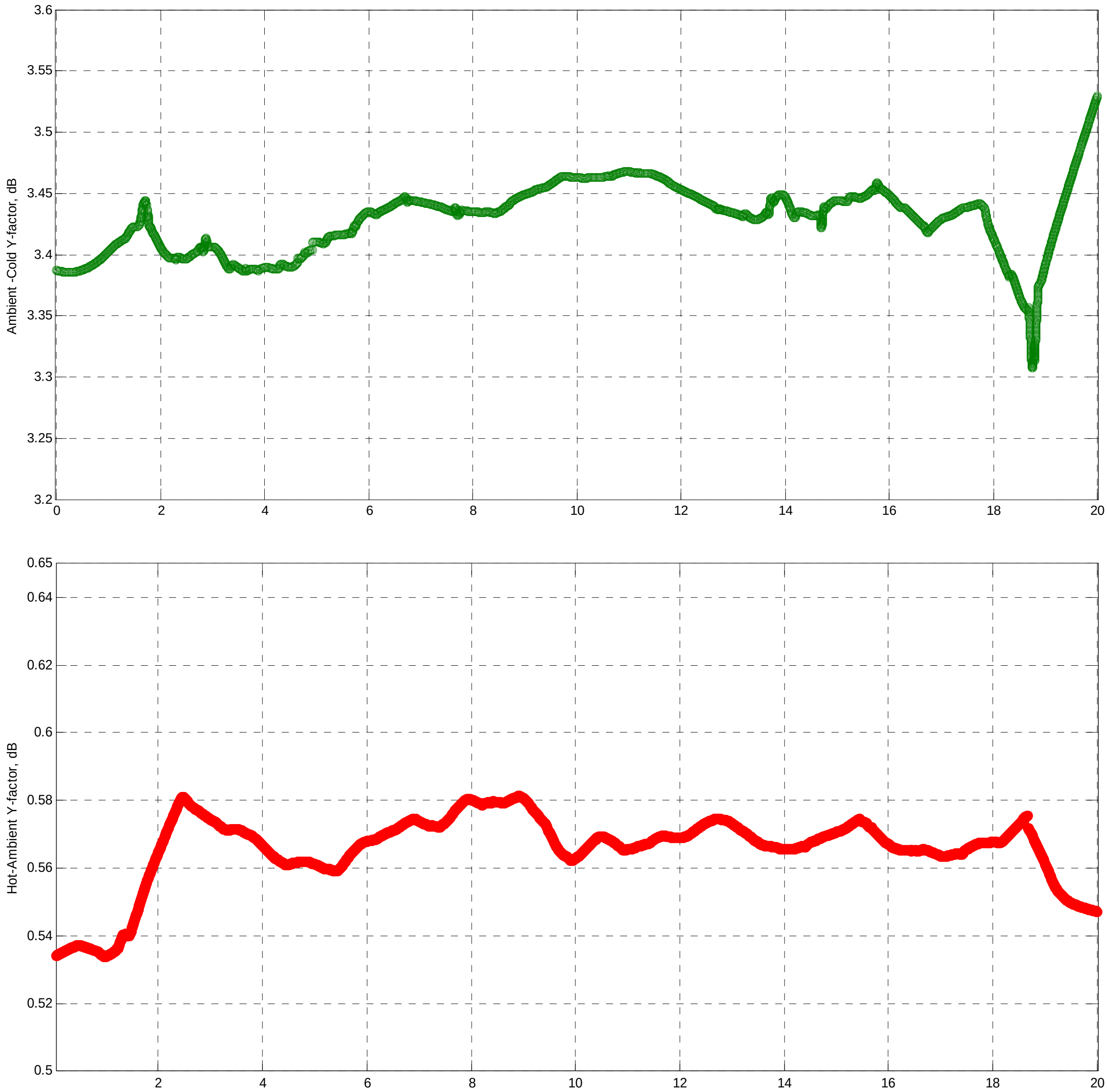

Figure 5-15. Band 9 test. Upper panel - IF output power for three loads: ALMA HCL, hand-held flexible Eccosorb at ambient (~23C) and LN2 cooled. Tilt table moved 0-90-0 degrees in 10 degrees steps. At each step three calibration loads were used. Middle panel – derived Y-factor for Ambient-Cold. Lower panel – Y-factor for Hot-Ambient.

Test 3.

Another Band 9 test. This time the tilt table moved from 0 to 90 degrees in one move, stayed there and moved back to 0 degrees. Results are presented in Figure 5-16.

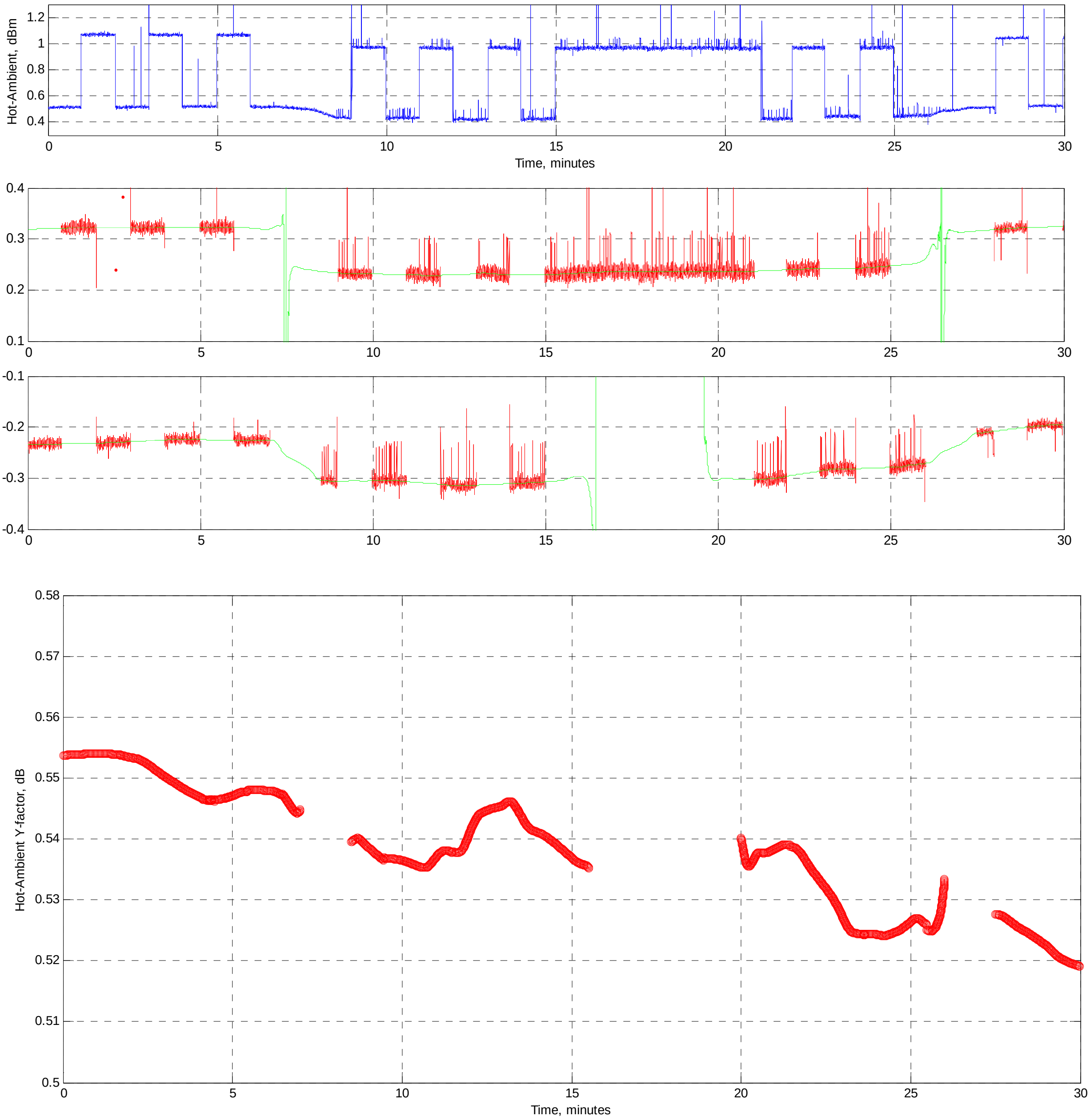

Figure 5-16. Band 9 test. Upper panel - IF output power for two loads: ALMA HCL and hand-held flexible Eccosorb at ambient (~23C). Tilt table moved 0-90 degrees in one move (~ 6-th minute) and then back (~27-th minute).

Test 4.

Yet another Band 9 test. Similar to Test 3, but with locked LO. Substantial drift might be because the LO system, including LORTM, did not have enough time to stabilize.

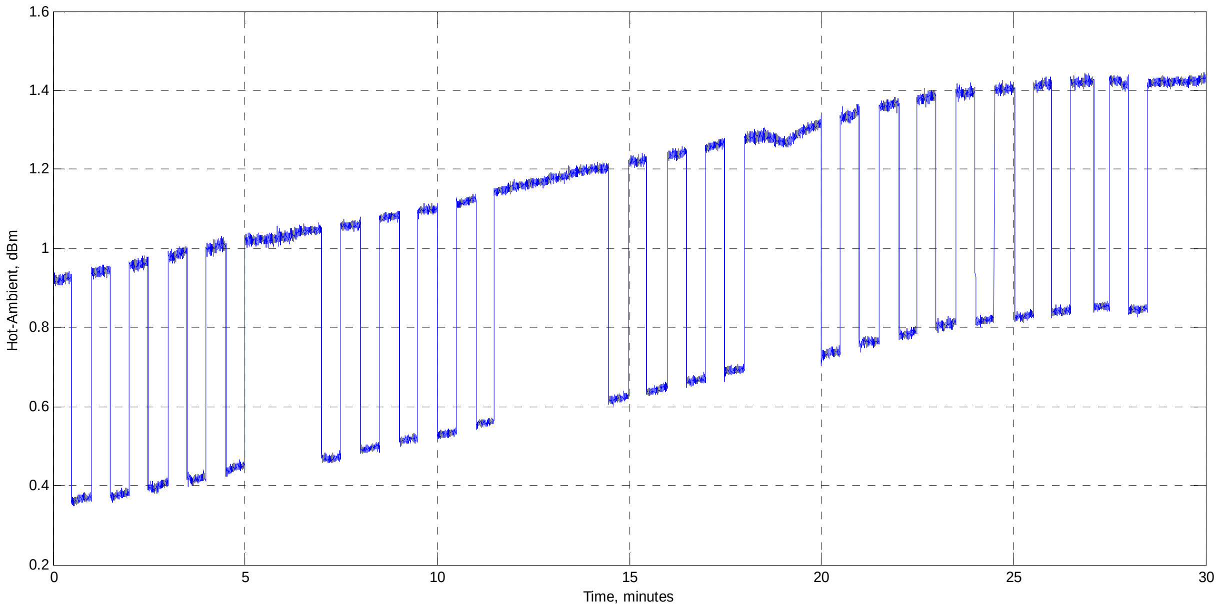

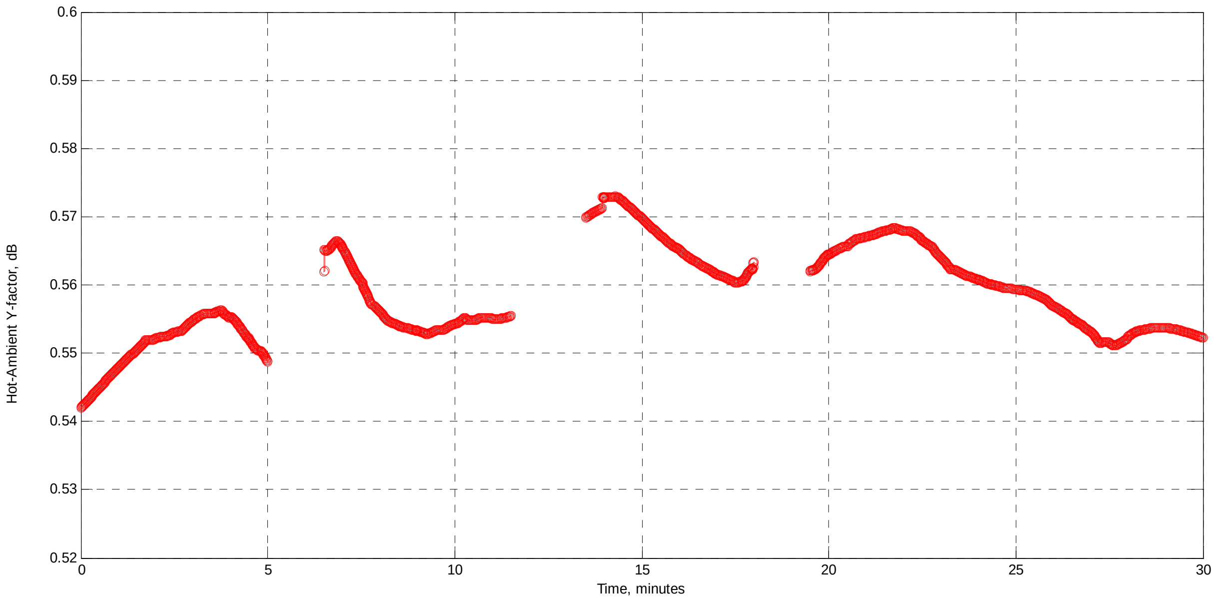

Figure 5-17. Band 9 test. Upper panel - IF output power for two loads: ALMA HCL and hand-held flexible Eccosorb at ambient (~23C). Tilt table moved 0-90 degrees in one move (~ 5-th minute) and then back (~18-th minute).

Test 5
Band 9, and two ambient loads used: ALMA Ambient, placed in front of the receiver, and soft Eccosorb, hand-held. ALMA ambient load is usually a few degrees warmer due to thermal coupling to the hot load via common mounting plate and also radiation. Room temperature in the lab is ~23 degrees,
controlled.

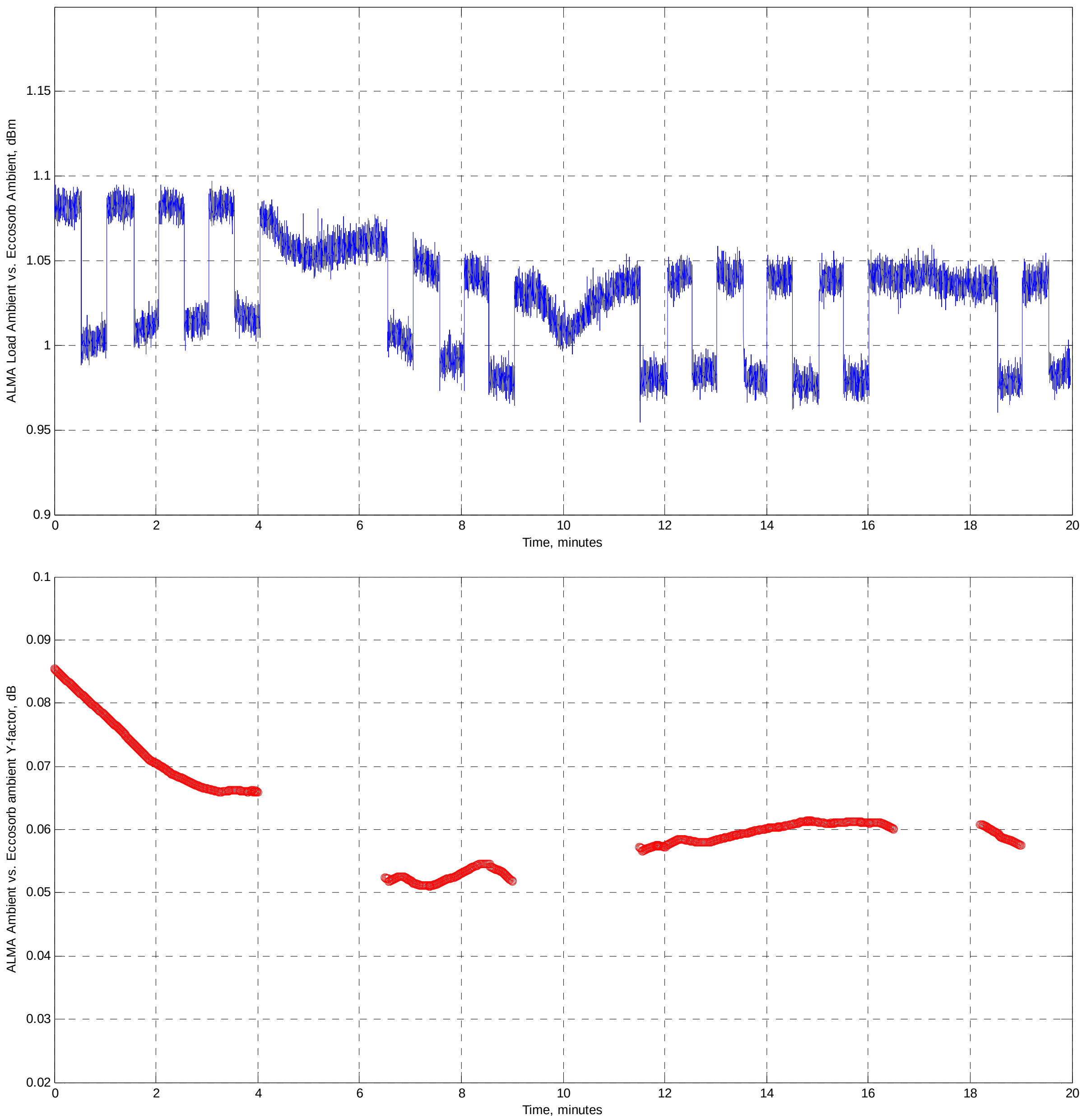

Figure 5-18. Band 9 test. Upper panel - IF output power for two loads: ALMA ACL and hand-held flexible Eccosorb at ambient (~23C). Tilt table moved 0-90 degrees in one move (~ 4-th minute) and then back (~9-th minute).

5.4. Effective temperature of the Loads as a function of tilt using both ambient and hot loads

In June 2010 more tests have been done at the EU FEIC using the hot and ambient prototype loads. Configuration of the measurements setup is shown in the Figure 5-19. In this case, the load scanner allowed to move both the hot and also the ambient load in front of the ALMA receiver, in this case Band 6 has been used set at LO=221 GHz. A third load, AN-72 folded into a cone dipped in liquid nitrogen, has been used to calibrate receiver gain. All measurements reported in this section were performed with the receiver phase locked, the measurements were taken by the FFTS back-end and averaged over a full 4-12 GHz IF bandwidth.

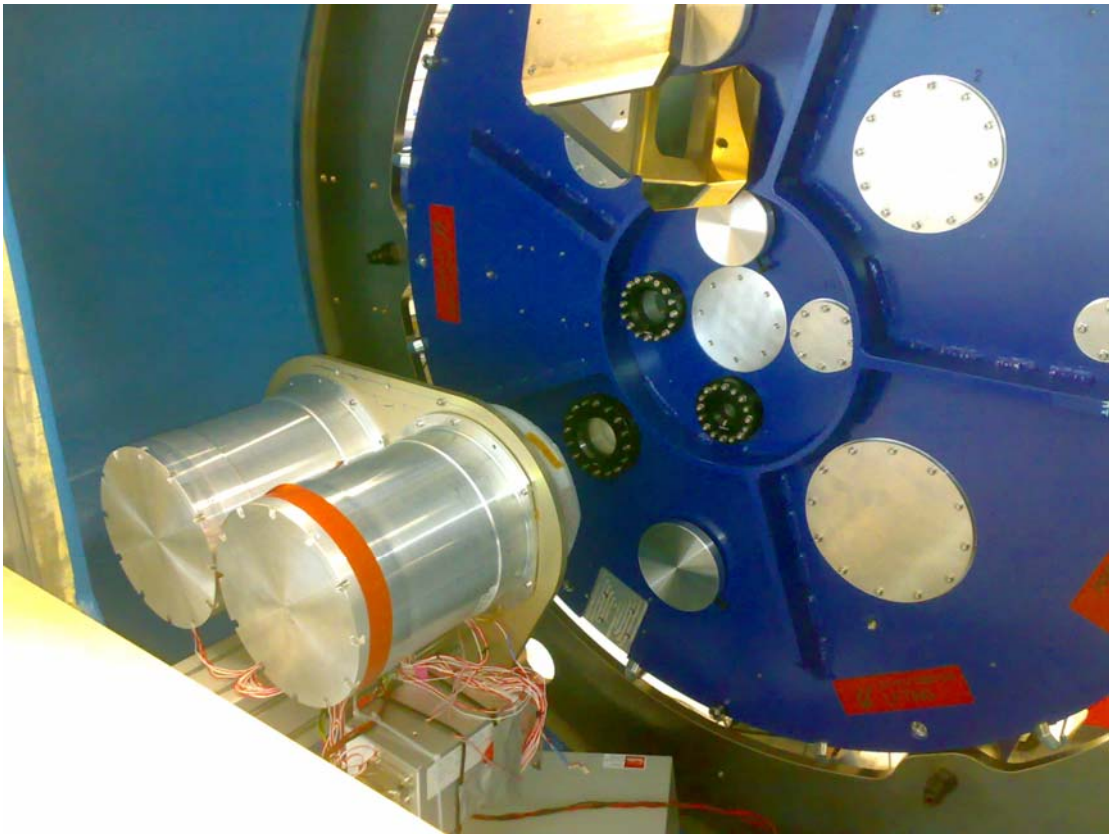

Figure 5-19. The load scanner allowes to move both the hot and the ambient load in front of the ALMA Band 6 receiver. A third load, AN-72 folded cone dipped in liquid nitrogen, is used to calibrate receiver gain, not shown in this picture.

Figure 5-20 shows results of the derived hot load temperature from the measured IF power levels with cold, ambient and hot loads in front of the receiver. Eight tilt angles, from 0 to 90 degrees with 15 degrees increments, were set in the measurements in random order. In order to allow the system to come to equilibrium, the measurements were taken with ~3 minutes delay after the next tilt angle has been introduced. The measurements accuracy is estimated to be ±0.5K (±0.01dB in the measured power levels). One of the error sources is uncertainty in the receiver gain calibration; due to in general not very well reproducible cold load. In order to address this error, one can assume (subject to error as well) the receiver gain to be independent of tilt and use only one, averaged value for the gain. Two sets of data are presented in the Figure 5-20: using the individual receiver gain calibration for each elevation, and also using the one averaged across all measurements. As one can see, there is no obvious tilt dependence of the derived hot load temperature within this error bar. The absolute scale is not calibrated for the receiver compression.

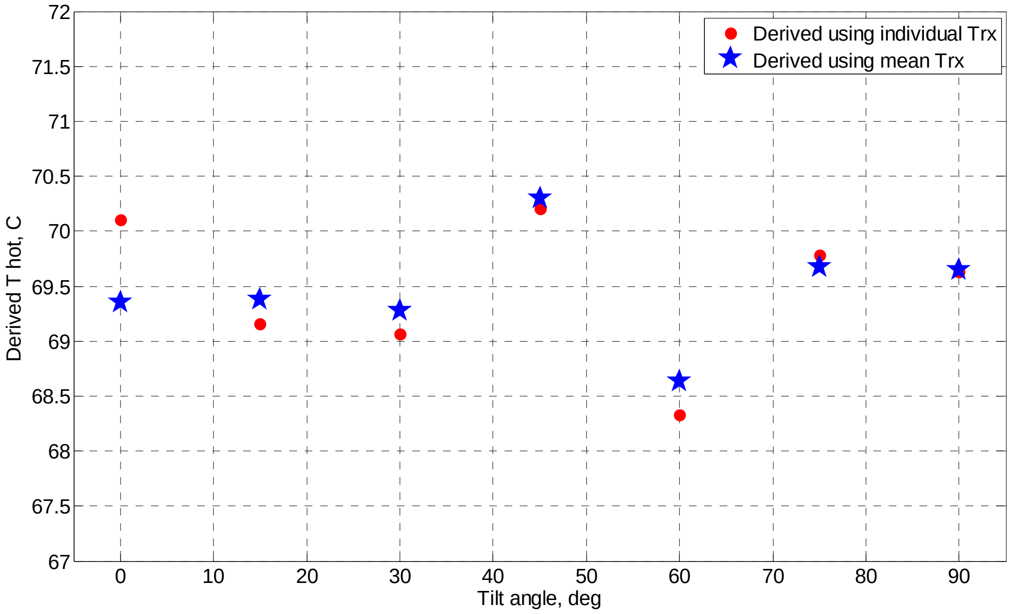

Figure 5-20. Derived hot load temperature using three loads technique. The ambient and cold data were used to establish receiver gain, and the pair of hot and ambient to derive hot load temperature from the receiver gain and ambient temperature. Two sets of data are presented: using the individual receiver gain calibration for each elevation, and also using the one averaged across all measurements. No correction was made for the receiver compression.

Acknowledgments.
EU FEIC team is acknowledged for their support in these measurements.

5.5. Conclusions

The radiometric measurements indicate an offset in the order of -0.5 K between the measured radiometric temperature and physical temperature of the Main Absorber. This is consistent with the thermal analysis of the HCL design in [RD2] and the measured temperature gradients in Section 3 of this report.

Besides the true calibration bias of the HCL the observed temperature offsets will be affected by all other element in the calibration chain. This includes a potential difference between the true radiometric temperature of the ACL and its temperature readout, especially since it was closer to the hot HCl aperture than it is under normal operating condition in the ACD. Another important error source is the LN2 cold reference, which is needed to establish the effective temperature of the noise diode. No corrections were applied to take scattering or temperature gradients of the LN2 target into account. For that reason we have most likely underestimated its temperature. This must results is an, although smaller, overestimation of our derived HCL temperature.

Effective radiometric temperature of the Hot Load has been measured using Band 9 receiver. It has no measurable bias with respect to its physical temperature monitored by the temperature sensors. The largest uncertainty remains in the effective temperature of the LN2 load.

Radiometric performance of the Hot Load as a function of tilt has been measured using Band 3, Band 6 and Band 9 receivers. No systematic variations, in the full range of 0-90 degrees tilt, have been found given an accuracy of the measurements setup.

6. MECHANICAL CHARACTERISTICS

6.1. Mass

The measured mass of the prototype loads is:

ACL – 5.9 kg

HCL - 5.6 kg.

6.2. Design volume

The measured envelope of the calibration loads is 290 mm in length and 200 mm in diameter.